Multivariate climate field reconstructions using tree rings for the northeastern United States

Jessie K. Pearl[1,2,3*], Kevin J. Anchukaitis[4,2,1], Neil Pederson[5], Jeffrey P. Donnelly[3]

[1]Department of Geosciences, University of Arizona, Tucson, AZ 85721 USA

[2]Laboratory of Tree-Ring Research, University of Arizona, Tucson, AZ 85721 USA

[3]Woods Hole Oceanographic Institution, Woods Hole, MA 02543 USA

[4] School of Geography and Development, University of Arizona, Tucson, AZ 85721 USA

[5] Harvard Forest, Harvard University, Petersham, MA 01366 USA

Key Points:

- Atlantic white cedar tree-ring chronologies are used for field reconstruction of northeastern United States temperatures.
- Atlantic white cedar growing in ombrotrophic environments are significantly correlated with precipitation, not temperature.
- Current temperature and precipitation trends are unlike those seen in the multicentury climate reconstructions.

* Corresponding author: Jessie K. Pearl, jpearl@email.arizona.edu

This article has been accepted for publication and undergone full peer review but has not been through the copyediting, typesetting, pagination and proofreading process which may lead to differences between this version and the Version of Record. Please cite this article as doi: 10.1029/2019JD031619

Abstract

High-resolution paleoclimate records are essential for improving our understanding of internal variability and the detection and attribution of forced climate system responses. The densely populated northeastern United States is at risk from increasing temperatures, severe droughts, and extreme precipitation, but the region has limited annual and seasonal-resolution paleoclimate records beyond the instrumental record. *Chamaecyparis thyoides*, L. (B.S.P.), Atlantic white cedar, a wetland conifer found within 200km of the Atlantic coastline of the United States, provides a promising tree-ring proxy that can fill in these data gaps. Here, we develop and analyze a new network of Atlantic white cedar tree-ring chronologies across the northeastern United States and demonstrate that site selection is important for regional paleoclimate reconstructions. Ring width variability reflects winter through summer temperatures at inland and hydrologically stable sites in the northernmost section of the species' range. Ombrotrophic sites along the coast record hydrological signals and correlate with growing season precipitation. We demonstrate skillful regional climate field reconstructions for the last several centuries and show the increased skill from incorporating our moisture sensitive sites into broad-scale products like the North American Drought Atlas. This comprehensive understanding of the species' climate responses leads to a tree-ring network that provides the long-term multivariate climate context at multidecadal and centennial time scales for the large-scale ocean-atmospheric processes that influence the climate of the region. We use this network to examine the covariance of temperature and drought across the New England area over the past two centuries.

1 Introduction

Anthropogenic climate change in the northeastern United States (hereafter, the 'Northeast') will have significant consequences for human health and the economic, cultural, and ecological resources of the region (Horton et al., 2014; Huang, Winter, Osterberg, Horton, & Beckage, 2017; Janowiak et al., 2018; Limaye, Vargo, Harkey, Holloway, & Patz, 2018; Pederson et al., 2013). Climate impacts are anticipated to be greatest in the densely populated urban New York to Boston coastal corridor (Brown, Bradley, & Keimig, 2010; Horton et al., 2014). The region, spanning from New Jersey to Maine, has already seen over a 1°C increase in annual temperature (Horton et al., 2014; Kunkel et al., 2013) and rapid step-wise increases in precipitation over the past century, which have been attributed

to increasing anthropogenic CO_2 (Howarth, Thorncroft, & Bosart, 2019; Pederson et al., 2013). These forced trends may, however, mask or incorporate important patterns of internal climate system variability that will continue to influence decadal-scale temperature and precipitation in the Northeast (Fischer & Knutti, 2015; Min, Zhang, Zwiers, & Hegerl, 2011; Pederson et al., 2013). Midlatitude and polar circulation anomalies, for example, have caused extremely cold winters in the past decade (Ballinger, Allen, & Rohli, 2014; Kretschmer et al., 2018), despite overall regional warming trends. Furthermore, increasing precipitation across the region cannot be fully explained by sea surface temperatures or atmospheric pressure patterns (Brown et al., 2010; Findell & Delworth, 2010; Groisman et al., 2004; Karl & Knight, 1998; Kunkel, Andsager, & Easterling, 1999; Min et al., 2011; Pederson et al., 2013; Seager, Pederson, Kushnir, Nakamura, & Jurburg, 2012). Intrinsic uncertainties regarding future forced climate change and the role of regional internal variability underscores the necessity to understand multidecadal to centennial climate variability across the region.

Developing paleoclimate temperature reconstructions for the Northeast is challenging due to the relative paucity of high-resolution temperature-sensitive proxy records in the region (Anchukaitis et al., 2017; Marlon et al., 2017; Trouet et al., 2013; Wilson et al., 2016). Tree-ring chronologies provide annual or sub-annual resolution information, can extend many hundreds of years or more into the past, and are effective proxies for climate variability and change over a wide geographic range, particularly in the mid-latitudes. In the Northeast, however, tree-ring chronologies typically exhibit mixed moisture and temperature responses, and are limited in age due to both widespread deforestation for agriculture and the short life span of most regional species (Conkey, 1979; E. Cook & Jacoby, 1977; Meko, Cook, Stahle, Stockton, & Hughes, 1993; Pederson, Cook, Jacoby, Peteet, & Griffin, 2004a; St George & Ault, 2014). These limitations present the largest challenge for statistically robust, multicentennial temperature reconstructions for the region. Northeastern trees have been used successfully, however, for drought and streamflow reconstructions (e.g. E. Cook & Jacoby, 1977; E. Cook & Krusic, 2004, 2012; Maxwell et al., 2017; Pederson et al., 2013). The North American Drought Atlas (NADA; E. Cook & Krusic, 2004, 2012) is a reconstruction of annual resolution, 0.5°x 0.5°gridded summer (June through August; JJA) Palmer Drought Severity Index (Palmer, 1965, PDSI) over the North American continent. This index of soil moisture can extend up to 2000 years in parts of western North America and has been used extensively to observe and

analyze drought patterns and variability across the United States (B. I. Cook, Ault, & Smerdon, 2015; B. I. Cook et al., 2016; E. Cook & Krusic, 2004; E. Cook, Meko, Stahle, & Cleaveland, 1999). In the Northeast, however, the NADA extends back only to the late 15th century, the tree-ring network that informs the drought reconstructions are primarily inland rather than coastal, and NADA does not use AWC (Figure 1).

Atlantic white cedar (*Chamaecyparis thyoides*, L. (B.S.P.), hereafter 'AWC') is a shade semi-intolerant tree species that lives in wetlands ranging from the Gulf of Mexico to Maine and no more than 200 kilometers distant from the coast (Gengarelly & Lee, 2006; A. Laderman, 1989). AWC was heavily harvested to make shingles, furniture, and boats until the 19th century (S. Little & Garrett, 1990). Regional differences exist in the species genetic makeup (Mylecraine, Kuser, Smouse, & Zimmermann, 2004), regeneration potential (Mylecraine, Kuser, Zimmermann, & Smouse, 2005), hydrological boundary conditions (Crawford, Day, & Atkinson, 2007; A. Laderman, 1989), and preferred substrate (Crawford et al., 2007). In the Northeast, AWC is typically restricted to areas too wet or anoxic for other species, and spends the majority of the growing season in standing fresh water environments (Kelsey, Joseph, & McWilliams, 2011; A. Laderman, 1989; Motzkin, 1990; NHESP, 2007). AWC has previously seen limited use for climate reconstructions, with recent work showing that in the northern extent of the species' range, reliable access to fresh water results in a positive growth response to temperature (Hopton & Pederson, 2005; Pearl, Anchukaitis, Pederson, & Donnelly, 2017). AWC therefore appears to be unique among Northeast species since it can be used to skillfully reconstruct temperatures across New England based on the widths of its annual rings (Hopton & Pederson, 2005; Pearl et al., 2017; Pederson, Cook, Jacoby, Peteet, & Griffin, 2004b). This temperature sensitivity is in contrast to *Taxodium distichum* (L.) Rich., a wetland tree species of the Gulf of Mexico and mid-Atlantic coast, which, despite its similar wetland habitat, has a significant relationship with spring-summer precipitation (D. Stahle, Fye, Cook, & Griffin, 2007), not temperature. Prior to this study, the hydroclimate sensitivity of AWC has not been explored in the Northeast for potential drought or precipitation reconstructions. We show that some AWC sites have a strong precipitation sensitivity in their ring widths link to their local hydrological setting. Here we use a network of recently collected AWC (Figure 1) across the Northeast to generate annually resolved, multicentury temperature and hydroclimate reconstructions, and improve the resolution of the NADA along the Northeastern seaboard.

Our new climate reconstructions provide opportunities for analysis of the spatial and temporal patterns of northeastern climate phenomena and their link to large-scale forcing. To demonstrate the utility of our northeastern multivariate climate field reconstructions, we examine one of the most anomalous regional climate events of the past 100 years: the 1960's drought (Namias, 1966, 1983; Seager et al., 2012). This drought was the most spatially extensive and persistent (lasting almost the entire decade) of the instrumental record, and in contrast to the 'hot droughts' seen in the western United States (Belmecheri, Babst, Wahl, Stahle, & Trouet, 2016; Berg & Hall, 2017; Griffin & Anchukaitis, 2014), coincided with abnormally cold temperatures for the entire decade (Namias, 1967; Seager et al., 2012). Current northeastern temperature and precipitation trends could be masking the potential for a severe droughts and altering the risk for their return (Newby, Shuman, Donnelly, Karnauskas, & Marsicek, 2014; Pederson et al., 2013; Sweet, Wolfe, DeGaetano, & Benner, 2017). We use our temperature reconstruction and an updated NADA drought reconstruction to observe the spatial fingerprint of frequency of these 'cold drought' events in the multi-centennial context.

2 Methods

2.1 Study Sites and Chronology Development

We sampled thirty-four AWC sites throughout the Northeast between 2014 and 2017 (Figure 1). Six of these sites (sites 2, 3, 17, 19, 21, and 24 in Table 1) were recollections of sites sampled by Hopton and Pederson (2005), and 28 sites are collections of previously unsampled AWC forests. Twenty-four sites north of 41°N with at least 100 years of tree-ring data were retained for paleoclimate analysis and reconstruction (Table 1) based on the latitudinal pattern of climate sensitivity identified by Hopton and Pederson (2005) and Pearl et al. (2017). At all sites, AWC was canopy-dominant and mostly even-aged. There are, however, large variations in the hydrological characteristics of the AWC wetlands throughout the Northeast. Many sites have 0.5 meters or more of standing water throughout the year and are fed by a nearby freshwater source such as a lake or stream. These 'hydrologically stable' sites, wetlands with consistent access to fresh water, are typically homogeneous stands with an understory of *Sphagnum* moss and fern species. Other AWC swamps are topographically higher, or geographically isolated from consistent fresh water sources. These 'drought prone' sites have minimal standing water and are apt to desiccate during droughts or from a change in hydrological regime due to nearby devel-

opment (A. Laderman, 1989; Laidig & Zampella, 1999; Motzkin, 1990; Rodgers, Day, & Atkinson, 2003). Drought prone swamps often have thick understory cover (plants such as *Rhododendron*) and often share the canopy with red maple (*Acer rubrum*, L.) and red spruce (*Picea rubens* Sarg.) around the periphery. We used exposed roots and elevated hummocks in the AWC swamps as indicators of past desiccation in these environments.

We propose a third hydrologic distinction for northeastern AWC sites that inhabit kettle holes along the coast; the 'ombrotrophic' sites. These glacial features are abundant in many northeastern coastal landforms, including as Cape Cod and Long Island (A. Laderman, 1989; Motzkin, 1990). In these acidic and anaerobic swamps, AWC often preferentially out-competes other wetland species, creating geographically confined and homogeneous stands (Golet & Lowry, 1987; A. D. Laderman, 1981). The thick clay till (fine-grained glacial diamicton) that underlies these coastal wetlands prevents groundwater from entering the swamps (Drake, 1971; Mulligan & Uchupi, 2003; Trettin, Jurgensen, Grigal, Gale, & Jeglum, 1996). These sites are not bogs, as is common for many ombrotrophic environments, but like ombrotrophic bogs they are dependent on precipitation and highly localized runoff for fresh water, aeration, and nutrients.

We collected increment cores of AWC following standard dendrochronological techniques (Fritts, 1976; Stokes & Smiley, 1968), taking 2 to 3 increment cores per living, mature, and canopy dominant tree and 20 to 40 trees per site. The cores were then dried, mounted, and sanded with progressively finer grit to reveal fine wood anatomical structure. To ensure we assigned the correct year to each annual ring, the increment cores were graphically and visually crossdated at each site (Stokes & Smiley, 1968; Yamaguchi, 1990). We measured ring widths at 0.001 mm precision and crossdating was statistically verified using the program COFECHA (Holmes, 1983).

To remove the geometric growth trend and isolate the common climate signal in the tree-ring series of each site, we detrended and standardized the ring width measurements into site chronologies. We used a standard negative exponential or linear growth curve (NEGEX) to retain low frequency climate signals (Fritts, 1976) based on the experiments by Pearl et al. (2017). Previous work testing the sensitivity of northeastern AWC ring-width series to different detrending techniques showed that the time series are susceptible to artifacts when using signal free detrending (Pearl et al., 2017), a standardization technique developed to attempt to avoid possible trend distortion or end effects

related to the presence of common medium-frequency variability (Briffa & Melvin, 2011; Melvin & Briffa, 2008). To account for changes in the number of series back in time, we stabilized the variance in the chronologies based on the interseries correlation (E. R. Cook, Briffa, Meko, Graybill, & Funkhouser, 1995) and a 67% spline (E. Cook & Peters, 1981, 1997; T. J. Osborn, Briffa, & Jones, 1997). For climate analysis and reconstruction, we only used the site chronologies when the expressed population signal was above the traditional threshold of 0.85 (T. J. Osborn et al., 1997; Wigley, 1984). We used the autoregressive (AR)-standardized version of the chronologies for our climate analysis and reconstructions to preserve the common autocorrelation structure of the tree-ring data believed to be due to variations in climate (E. Cook, 1985). We used the Blackman-Tukey method (D. B. Percival, Walden, et al., 1993) to classify the spectral and auto-correlation properties of each site. To ensure that the calculation of these spectral properties of the AWC chronologies were not dominated simply by the pervasive warming and wetting trends in the Northeast, we preformed a sensitivity test by comparing the AWC time series characteristics before and after removing the 21st century trend, as well as before and after truncating the time series at 1970.

2.2 Climate Analysis

We extracted the local grid point monthly temperature data from the Climate Research Unit (CRU) TS4.01 temperature product (Harris, Jones, Osborn, & Lister, 2014) and monthly precipitation data from version 7 of the Global Precipitation Climatology Center (GPCC) precipitation product (Schneider et al., 2016) at each AWC site to analyze the site's climate response. We calculated temperature anomalies from the 1950-1980 mean temperatures. We performed seasonal correlation analyses as described by Meko, Touchan, and Anchukaitis (2011) to calculate both the Pearson correlation and partial correlation coefficients of the chronologies with monthly and seasonal temperature and precipitation. Statistical significance of the seasonal correlations was evaluated using exact simulation (Meko et al., 2011; D. Percival & Constantine, 2006).

To distinguish site-specific and broad-scale climate responses across the network, we performed an empirical orthogonal function (EOF) analysis on the entire network and on the AWC sites identified in our seasonal correlation analysis to be significantly correlated ($p < 0.01$, the 'high sensitivity' sites) with temperature or precipitation. We correlated the time series expansion of the leading EOFs with January-August mean tem-

perature (CRU TS4.01, Harris et al., 2014; Pearl et al., 2017) and March-August precipitation (GPCC, Schneider et al., 2016) fields to assess the extent of spatial correlation suitable for field reconstruction (Bretherton, Smith, & Wallace, 1992; Meko et al., 2011; D. Percival & Constantine, 2006; Wallace, Smith, & Bretherton, 1992). We analyzed the spatial loadings of the leading EOFs of the high sensitivity sites with respect to our field-based hydrological designations. To examine the influence of sea surface temperatures (SSTs) on the terrestrial climate variability that controls AWC growth, we compared the leading EOFs of the network against gridded sea surface temperatures from the UK Met Office Hadley Center (HADISST, Rayner et al., 2003).

2.3 Spatial Temperature Reconstruction

Based on the climate analyses described above (Figure 2A,C) and our prior findings (Hopton & Pederson, 2005; Pearl et al., 2017), we reconstructed January-August mean temperatures using the CRU TS4.01 temperature product as the gridded predictand over the area enclosed by 75°W to 67°W and 39°N to 48°N. Our site and network-level analysis yielded a set of 24 tree-ring chronologies (Table 1), and the chronologies lagged by one year with respect to climate, as predictors for the reconstruction models. Our use of lagged predictors was based on seasonal correlation analyses (Meko et al., 2011), and the significant autocorrelation in the AWC chronologies (Figure 3).

We used a point-by-point regression ('PPR') technique to reconstruct gridded January-August mean temperatures for the Northeast (Anchukaitis et al., 2017; E. Cook et al., 1999). This method sequentially fits single grid point principal component regression (PCR) models over a gridded field. Each grid point model is determined by the sets of predictors located within a 500km search radius. We pre-screened the tree-ring chronologies for significance at $p < 0.1$ level for entry into the predictor pool (E. Cook et al., 1999). Model selection is based on the Akaike Information Criterion (Akaike, 1974; E. Cook et al., 1999). Each grid point's reconstruction is nested so that as shorter chronologies drop out, a new PCR model is calculated and screened for significance with the remaining chronologies (Meko, 1997). This method allows for the reconstruction to vary in length back in time as dictated by the tree-ring chronologies within the search radius (E. Cook & Krusic, 2004; E. Cook et al., 1999).

We used a split calibration and validation procedure (using the periods 1900-1955 and 1956-2010) to train and evaluate our models (Meko, 1997; Michaelson, 1987), and used the full period (1900-2010) to calibrate the final reconstructions (Snee, 1977). We quantified the variance explained by our reconstruction using the R^2 statistic. We used the reduction of error (RE) and coefficient of efficiency (CE) statistics to estimate reconstruction skill, with positive RE and CE values indicating the reconstruction performed better than a naïve estimate of the mean (E. Cook et al., 1999; Wahl & Ammann, 2007). For further proxy-validation, we observe years of anomalous northeastern temperatures described in the historical record prior to the start of the instrumental record (c.f. E. R. Cook, Anchukaitis, et al., 2010; E. R. Cook, Seager, Cane, & Stahle, 2007). To determine the larger scale climate dynamics associated with northeastern climate anomalies, we defined the 75th (warmest) and 25th (coldest) percentile of the Northeast regional temperatures as reconstructed by the AWC network and composited the surface temperature, sea level pressure, and sea surface temperatures anomalies from the 20th Century reanalysis product for those years (Compo et al., 2011).

2.4 Precipitation and PDSI Reconstructions

Based on our site level and network climate analysis (Figure 2B,D), we used the ombrotrophic sites (Table 1) to reconstruct Southern New England March through August ('growing season') precipitation for the region from 41°to 42.5°N and 72°to 69°W extracted from the GPCC v7 product (Schneider et al., 2015). The area of highest correlation between the leading signal of the ombrotrophic sites and precipitation includes a relatively small region (Figure 2B) as coastal precipitation variability here is highly localized (Brown et al., 2010; Kunkel et al., 2013). We therefore used a simple nested composite-plus-scale (CPS) approach (E. Cook, D'Arrigo, & Mann, 2002; Esper, 2005; Esper, Cook, & Schweingruber, 2002; Pearl et al., 2017) to reconstruct precipitation for this specific region alone. This method scales the tree-ring series to the mean and standard deviation of the instrumental observations during the calibration period, and then evaluates the fit between tree-ring reconstructed total precipitation and the instrumental data during the validation period. We used a split calibration and validation (using the time period of 1925-1960 and 1961-2012) approach to train and evaluate our models (Meko, 1997; Michaelson, 1987). We estimated the uncertainty of our reconstructed time series using the root mean square error (RMSE) of validation. As above, we quan-

tify the reconstruction explained variance using the R^2 statistic, and use the RE and CE statistics to validate our models and estimate reconstruction skill (E. Cook et al., 1999; Wahl & Ammann, 2007).

Although a skillful northeastern field reconstruction of precipitation or PDSI is not possible using our limited number of ombrotrophic sites as predictors, these moisture sensitive sites do provide a new coastal source of paleoclimate data not present in the NADA. We therefore incorporate our ombrotrophic chronologies with the existing NADA chronologies (E. R. Cook et al., 2007; E. R. Cook, Seager, et al., 2010) to provide additional information for drought reconstruction at coastal gridpoints. We reconstructed the same JJA PDSI season that is reconstructed in the NADA, for the Northeast using 1) only the ombrotrophic AWC sites as predictors, and 2) both the ombrotrophic AWC sites and northeastern NADA sites. We used the PPR method described in section 2.3 using the 0.5°x0.5°CRU self-calibrating Palmer Drought Severity Index (T. Osborn, Barichivich, Harris, van der Schrier, & Jones, 2017; Wells, Goddard, & Hayes, 2004) as the gridded predictand. We use a split calibration and validation procedure and period to train and evaluate our models (Meko, 1997; Michaelson, 1987) and used the full available period covered by predictors and predictand for calibration in the final reconstructions (Snee, 1977). Many NADA chronologies terminate in 1980, thus limiting the number of common overlapping years between the ombrotrophic and NADA chronologies during the instrumental period. As such, our split calibration and validation period was adjusted to 1900-1940 and 1941-1980. We use the same statistical skill measures as described above.

Using our temperature field reconstruction and our combined Omborotrophic+NADA drought reconstruction we examined periods of anomalous climate in the Northeast. We extracted a regional PDSI average bounded by 75°W to 67°W and 40°N to 48°N from the reconstruction to identify periods of drought of two or more years when the regional average PDSI was -1 or less (E. Cook et al., 1999; Herweijer, Seager, Cook, & Emile-Geay, 2007; **?**). We calculated the duration of these droughts and quantified their spatial extent using the drought area index (DAI) metric (E. R. Cook, Seager, et al., 2010), which quantifies the percent of reconstructed grid points that are below a given threshold of PDSI (here, -1) at a given time. Using DAI, we identified droughts similar to the 1960's drought over the past two centuries and mapped the corresponding years' temperature field. We then generated composite temperature and PDSI maps for the periods of drought

identified in the Omborotrophic+NADA regional average in order to identify the association between temperature and moisture anomalies in the past.

3 Results

3.1 Climate signals and hydrogeological influences on climate-growth relationships

All AWC sites crossdate internally with interseries correlations between $r = 0.5$ and $r = 0.7$. The majority of our AWC network is significantly ($p < 0.05$) and positively correlated with local January-August temperatures (Figure 2C) and not significantly correlated with growing season precipitation (Figure 2D). The hydrologically stable sites have the highest correlations with local January-August mean temperature, while both drought-prone and ombrotrophic sites have weaker and mixed temperature and precipitation climate signals (Figure 2C, D). The non-ombrotrophic sites with the weakest temperature correlation, BVC and MAF, are two of the southernmost sites in the network. SAC has the highest correlation with local temperature, and is the only coalesced bog (formed by continuous peat accumulation in adjacent ponds, eventually connecting and growing together above the water table) in the network, and possibly the southernmost coalesced bog in the eastern United States (A. Laderman, 1989; Pearl et al., 2017). The leading mode of variance (EOF) of the AWC network explains 46% of the variance, and correlates with CRU TS4.01 (Figure 2A) January-August mean temperature field at $r \geq 0.5$ for the entire Northeast, and correlates with Gulf of Maine and near-shore SSTs at $r > 0.4$ west of 68°W (Figure 4). Correlation with the CRU TS4.01 January-August mean temperature field drops below $r = 0.3$ southeast of New York state (Figure 1, Figure 2A).

Our seasonal climate analysis of the ombrotrophic sites in Cape Cod (marked as triangles in Figure 2C and D), showed significant ($p < 0.01$) sensitivity to growing season precipitation. The leading mode of variance (EOF1) of the ombrotrophic network correlates with Cape Cod and coastal New England (south of 44°N) precipitation at $r > 0.5$ and above (Figure 2B). EOF1 of the ombrotrophic network has lower correlation with adjacent and Atlantic basin SSTs (Figure 4). The EOF analysis of the high sensitivity sites confirms this multivariate climate signal in the network. The hydrologically stable sites with a strong local temperature signal load strongest on the first EOF (46% of the

variance), and ombrotrophic sites along the coast load strongest on the second EOF (15% of the variance). The temperature sensitive chronologies have more persistent and stronger positive autocorrelation than the ombrotrophic chronologies (Figure 3). This is exceptionally pronounced when the 21^{st} century trend is included, but remains even when the recent growth trends are removed (Figure 3), suggesting this is characteristic of these sites even without recent warming. The ombrotrophic chronologies have more high frequency variance, mainly in the 4-6 year period, than the temperature sensitive network which is dominated by low frequency variability (Figure 3).

3.2 Temperature Field Reconstruction

We developed a skillful January-August gridded mean temperature reconstruction for the Northeast spanning the interval 1820-2013. Our reconstruction explains up to 47% of grid point temperature variance (Figure 5), however, not all gridpoints in the reconstruction have a stable reconstruction model through time, with statistical skill dropping to fewer gridpoints in the later 18th century. West of 78°W, north of 47.5°N, and south of 39°N, our reconstruction models do not pass cross calibration and validation procedures, with negative RE or CE in the reconstructions. The inclusion of 2011-2012 in our calibration period weakens the skill statistics of the reconstruction. Whether this reflects a threshold of temperature sensitivity of AWC is unclear from these data, but suggests an avenue for future investigation (Bunn, Salzer, Anchukaitis, Bruening, & Hughes, 2018).

To further validate the proxy reconstruction, we use our reconstruction to map years of known anomalously cold and warm temperatures outside the instrumental record. The 'Year without Summer', 1816, is a known cold period for the northern hemisphere following the eruption of Mount Tambora in 1815 (Anchukaitis et al., 2017; Chenoweth, 1996; Harington, 1992; Rampino & Self, 1982; Stothers, 1984). Our reconstruction shows widespread cooling of 1-3°C over most of New England compared to the 20th century average temperatures (Figure 6). This cooling persisted for two years, with 1816-1817 being one of the coldest periods in the Northeast over the entire reconstruction. To ensure that the reconstruction also represents pre-industrial warm years, we mapped temperature for January-August 1828 (Figure 6). Historical documents across New England suggest the winter and spring of 1828 to be abnormally warm, with February temperatures almost 4°C in excess of the 1820-1840 mean in some locations (Ludlum, 1966; Mock,

Mojzisek, McWaters, Chenoweth, & Stahle, 2007). Our reconstruction shows warming of January-August mean temperature up to 1°C compared to the 20th century average (1950-1980) reference period across the entire Northeast for that year. 1828 is one of the warmest years in our reconstructed temperature record before 1900 and these anomalies are even larger when comparing to the 1820-1840 reference period used in historical documents (Ludlum, 1966; Mock et al., 2007). Our reconstruction shows that the warming trend of the past 40 years in the Northeast is unique over the past two centuries, consistent with Pearl et al. (2017). Prior to 1970, the longest run of anomalously warm years was from 1858 to 1868, although these years were only slightly (at most 0.4°C) above the 1950-1980 average, whereas recent warming has seen January-August mean temperature anomalies over 2.5 °C.

Our comparison of the AWC temperature reconstruction with Reanalysis data (Compo et al., 2011) shows circum-Atlantic temperatures vary in association with broad scale winter sea level pressure patterns (Figure 7). Anomalously cold years in the Northeast cooccur with a negative winter North Atlantic Oscillation (NAO) pattern of atmospheric pressure, and warm years with a positive NAO pattern (Figure 7B) in the 20th century. Northern Europe, in particular Fennoscandia, shows concurrent years of anomalously warm and cold years with the Northeast.

3.3 Southern New England Precipitation and Coastal Drought Reconstructions

We generated a skillful multicentury reconstruction of March through August precipitation for the Southern New England and Cape Cod region using the local ombrotrophic sites (Figure 8). Our model has positive RE and CE scores of 0.31 and 0.29, respectively, and an R^2 value of 0.37 from 1828-2014. The model maintains skill (RE and CE scores of between 0.21-0.28, and R^2 values between 0.33-0.39) through the earliest 19th century. The reconstruction is stable through time back to 1802, when the RE and CE values drop below zero. Split calibration and validation testing showed that the precipitation reconstruction is sensitive to small shifts in the calibration time period when calibrating with the later period and validating with the earlier period. CE in particular is known to be sensitive to the calibration and validation period (Pearl et al., 2017; Wahl & Ammann, 2007; Wahl & Smerdon, 2012), and does not influence our overall confidence in the reconstruction. Early instrumental precipitation data used for the GPCC prod-

uct are relatively sparse which may account for some of the mismatch between our reconstruction and gridded observations in the 1910s and 1920s (Brown et al., 2010; Schneider et al., 2015). Our tree-ring reconstruction captures both inter-annual as well as multidecadal variability (Figure 8), including a period of continuous high precipitation from 1850-1900.

To improve the resolution of drought reconstructions along coastal New England, we included our ombrotrophic sites in a field reconstruction of PDSI across the Northeast. As expected, a gridded reconstruction of PDSI for the northeastern US using only the ombrotrophic sites shows skill only proximal to the predictors – over the same region where we are able to skillfully reconstruct precipitation using a CPS approach – for the period 1792-2014 (Figure 9, **S2**). When combined with the more abundant moisture-sensitive NADA chronologies, however, we are able to skillfully resolve drought over both the coast and islands of the Northeast that are not included in the NADA (Figure 10). Throughout the instrumental record, there are years where JJA PDSI fields disagree with the reconstructed fields in the NADA (Figure 10). These disagreements are most pronounced along the northeastern coast, where the NADA reconstructs a different magnitude, or even opposite sign, PDSI value than the target instrumental field (Figure 10). When we include the ombrotrophic sites as predictors along with local NADA sites in a PDSI reconstruction, we not only better resolve the missing coastal features, but more accurately represent coastal drought dynamics (Figure 10), demonstrating the value for future field reconstructions of drought from including ombrotrophic AWC chronologies in the northeastern United States.

During the 1960's, regional reconstructed PDSI was less than -1 from 1962-1970, and reconstructed regional January-August mean temperature anomalies were around -1°C or below across the Northeast from 1960-1971. The 1960's drought had an average DAI value of 48%. Over the past 200 years, five reconstructed droughts were similarly widespread across the region, and two of those droughts were decadal in length like the 1960's drought. Using our multi-centennial records of Northeast temperature and drought, we see that periods of cold are typically contemporaneous with periods of drought (Figure 11, Figure S1). Our reconstructions indicate that cold droughts are common features of the past two centuries, with the most prolonged droughts in the Northeast averaging 0.25-0.75 °C colder than the 20th century mean across the entire region (Figure 11 B).

4 Discussion

In contrast to arid sites in western North America or high latitude sites along the northern treeline, tree-ring reconstructions in the northeastern United States – particularly of pasts temperatures – are challenging due to the mixed and diverse climate response of species across the region. Uncertainties in paleoclimate reconstructions here arise from these complex climate responses, the distribution of chronology sites, and the relatively short lifespan of more species in the Northeast (Alexander et al., 2019; Anchukaitis et al., 2017; E. R. Cook & Pederson, 2011; Marlon et al., 2017; Meko et al., 1993; Pederson et al., 2004a; Trouet et al., 2013; Wilson et al., 2016). As a consequence, previous work using tree-rings as paleotemperature proxies has been limited to regional average reconstructions (Pearl et al., 2017) or reconstructions targeting local weather stations (Conkey, 1979), rather than field reconstructions. Spatial reconstructions are powerful tools that allow for comprehensive understanding of regional climate characteristics, evaluate the influence of different forcings on the climate system, and provide insight into regional climate patterns in response to large-scale modes of ocean-atmosphere variability (E. R. Cook, Anchukaitis, et al., 2010; E. R. Cook, Seager, et al., 2010; Goosse, 2017; Phipps et al., 2013). Our use of AWC as a paleotemperature proxy results in a skillful field reconstruction of temperature for the Northeast using a regional network of tree-ring chronologies. If these chronologies can be extended further in time, they potentially fill an important gap in large-scale temperature field reconstructions for the Northern Hemisphere (Anchukaitis et al., 2017).

There is a clear latitudinal influence on temperature correlation of AWC sites, with weaker correlations at the southernmost and more drought prone sites (Figure 2). This confirms the relationship between latitude and temperature sensitivity shown by Pearl et al. (2017), as well as the tendency for the growth of trees in the eastern U.S. to be limited by moisture, not temperature, away from the boundaries of their ranges (E. Cook & Jacoby, 1977; Graumlich, 1999; Pederson et al., 2013, 2012; D. W. Stahle & Cleaveland, 1992). Our analysis here, however, shows that the hydrological conditions of the sites can overwhelm this latitudinal trend, as the sites with the highest temperature correlations are not necessarily the northernmost sites. Rather, the sites with the strongest temperature correlation are those in hydrologically stable wetlands, above 41°N (Figure 2). The site with the highest correlation, SAC, is located in a raised bog with an elevated water table, which may play into its heightened temperature correlation.

Due to the unique geohydrology of the ombrotrophic sites, the climate response of the AWC trees at these sites are distinct from the rest of the network. Our network analysis shows that AWC in ombrotrophic swamps have statistically significant correlations with growing season (March-August) precipitation, and much lower correlation with local temperatures and SSTs (Figure 4). The relationship with local precipitation allows us to successfully reconstruct growing season precipitation for Southern New England. Additionally, our results show that we can also use these ombrotrophic AWC sites to provide novel information on coastal New England PDSI that is not captured in the NADA (E. R. Cook, Seager, et al., 2010), and thus improve the drought reconstructions for the area. We do not find a response to winter precipitation, which suggests that snowfall plays an insignificant role in growth compared to the amount of freshwater received from precipitation during the growing season. Not all of the ombrotrophic sites, however, are simple precipitation proxies. MRC, for example, is significantly correlated ($p < 0.01$) with local January-August temperatures as well as with growing season precipitation. Additionally, not all sites in Quaternary outwash deposits (such as Cape Cod) are ombrotrophic; temperature sensitive AWC sites, such as MPB or ELL, exist in glacial outwash that are fed by nearby ponds or streams, and are not isolated in depressed basins. We have used these hydrological distinctions between sites in our study to offer a physical explanation why certain coastal AWC sites have insignificant temperature correlations, and strong precipitation growth responses. Persistent and significant autocorrelation appears to be characteristic of those sites with a dominant temperature signal in their annual ring widths (Figure 3). This is in agreement with ecological studies of western canopy dominated forests, where low-frequency variations reflect temperature fluctuations and the high-frequency fluctuations reflect precipitation variations (e.g. Lamarche, 1974). Sites that are moisture sensitive tend to have lower, less persistent lagged correlation, and more pronounced variability in the 3-10 year frequency (Figure 3). This information is also useful for identifying the climate response of subfossil 'ghost forests' that can be used to extend the living tree chronologies from the region.

Our gridded northeastern temperature reconstruction can be used to confidently identify temperature patterns back to 1820 C.E., with the highest confidence in coastal New England (Figure 5). Skill at many grid points declines in the early 1800's, as we lose the majority of our predictor chronologies (Table 1). Although not all grid points pass traditional thresholds for skillful split sample calibration and validation RE and CE,

our reconstruction nevertheless still confirms historical years of anomalous temperatures in the early 1800's (Figure 6). In years of extreme temperature anomalies, the region experiences widespread temperature changes of the same sign (Figure 6). This is in contrast to our drought reconstruction, where we see clear spatial distinction between inland and coastal PDSI even in years of large regional-scale drought anomalies (Figure 10). The abundance of ombrotrophic AWC sites on Cape Cod allow us to skillfully reconstruct southern New England precipitation back to the early 18th century (Figure 8), but not much of the the rest of the Northeast (Figure 9). Nevertheless, the coastal ombrotrophic AWC more accurately represent northeastern coastal drought than the NADA (Figure 10), and by combining the ombrotrophic sites with the NADA predictors we can resolve the fine coastal features of the Northeast, and improve regional hydroclimate and drought reconstructions (Figure 8, Figure 10).

The majority of the AWC network is located less than ten kilometers from the coast, where climate is strongly influenced by Atlantic Ocean dynamics (B. I. Cook, Cook, Anchukaitis, Seager, & Miller, 2011; Feng, Beighley, Hughes, & Kimbro, 2016; Namias, 1967; Seager et al., 2012; Wettstein & Mearns, 2002). We find strong correlations with the temperature sensitive network's EOF1 with local and cross basin Atlantic SSTs (Figure 4) (Pearl et al., 2017). The ombrotrophic sites have much lower correlations with SSTs, indicating that local ocean temperatures may have a stronger influence on regional surface air temperature than southern New England hydroclimate. Our precipitation reconstruction shows persistent, elevated moisture from approximately 1850 to 1900 (Figure 8) corresponding to a period of warm Atlantic SSTs (a positive Atlantic Multidecadal Oscillation index) (Enfield, Mestas-Nunez, & Trimble, 2001; Hu, Feng, & Oglesby, 2011). The AWC network as a whole provide information about variability in local western North Atlantic sea surface temperatures and basin-scale atmosphere circulation (Anchukaitis et al., 2019; Pearl et al., 2017). The 1960's drought, for example, corresponded with a negative phase of the NAO, and has been attributed to a combination of anomalously cold ocean temperatures off shore and internal atmospheric variability (Collins, 2009; Namias, 1966, 1967; Seager et al., 2012). This was the most recent period of sustained negative temperature anomalies across the entire Northeast, with comparable long periods of cold in the early 1900s (1899-1914), and early to mid 1800's (1806-1821). Both of these periods also correspond with dry conditions and increased DAI of 52% and 54%, respectively. Our results show that over the past 200 years most northeastern droughts of com-

parable duration and DAI to the 1960's were accompanied by cooler temperatures across the Northeast (Figure 11B). The most severe reconstructed droughts in the 20th century corresponded with cooler than average offshore SSTs (Figure 11 C). Reconstructions of the NAO (E. R. Cook et al., 2019; Jones et al., 1999) and the strong relationship of the temperature sensitive AWC network with Atlantic SSTs (Figure 4, Figure 7) lead us to infer that other periods of cold drought seen in our reconstructions beyond the period of instrumental data would also have been accompanied by a negative NAO phase (Anchukaitis et al., 2019; E. R. Cook et al., 2019; Jones et al., 1999) and cooler than normal nearshore SSTs (Figure 11, Figure 7). Our reconstruction shows a coherent temperature sensitivity across the Atlantic to broad scale winter NAO patterns (Figure 7) that is also observed in larger terrestrial proxy networks over the past millennium (Anchukaitis et al., 2019). This relationship allows for the potential to improve estimates of hemisphere-scale temperatures and atmospheric circulation anomalies based on our Northeastern reconstruction.

This study's gridded temperature reconstruction expands beyond single index reconstructions previously developed for the region (Conkey, 1986; Pearl et al., 2017). The reconstruction, however, remains limited by the young ages of the chronologies used here, highlighting the need for continued development of longer temperature sensitive tree-ring chronologies. Many of the longest chronologies in our network are ombrotrophic, which tend to have much weaker temperature signals than the hydrologically stable sites. The young ages of AWC across the Northeast is primarily a consequence of extensive harvesting of AWC wood that continued until the late 1800's. To generate longer paleoclimate records, preserved dead ('subfossil') wood can be used in combination with living material (Boswijk et al., 2014; Crawford et al., 2007; Grudd et al., 2002; Roig Jr, Roig, Rabassa, & Boninsegna, 1996; Salzer & Hughes, 2007; Salzer, Pearson, & Baisan, 2019; Wilson et al., 2012). The primary source of subfossil AWC exists along the northeastern coast line where ancient 'ghost forests' are now exposed in marsh and tidal environments (Bartlett, 1909; G. H. Cook, 1857; Heusser, 1949). Due to their proximity to, or location in, glacial outwash material, subfossil AWC may have grown in ombrotrophic environments. The differences in time series characteristics between the ombrotrophic and temperature sensitive chronologies (Figure 3), therefore, are important tools for distinguishing the likely climatic influences and geologic context of subfossil AWC. Subfossil AWC wood from the Northeast offers an opportunity to extend the length of temper-

ature reconstructions beyond what is possible using living trees alone (Bartlett, 1909; G. H. Cook, 1857; Gleba, 1978; Heusser, 1949; A. Laderman, 1989).

5 Conclusions

AWC is unique among northeastern trees as its annual growth at most locations is significantly correlated with winter through summer temperature. Our work shows that careful site selection is critical for climate reconstructions when using AWC as a paleoclimate proxy. Temperature sensitive sites are restricted to the highest latitudes of the species' range, and coastal sites in ombrotrophic swamps are moisture, not temperature, growth dependent. The ombrotrophic swamps in our study are restricted to Cape Cod, where they experience more temperate maritime temperatures than the inland sites (Brown et al., 2010; Horton et al., 2014), and in these environments their primary freshwater source is precipitation. These hydrological and geographical site conditions cause the ombrotrophic AWC tree-ring chronologies to be better suited for precipitation (Figure 8) and drought (Figure 10) reconstructions.

We use the temperature sensitive AWC to reconstruct a gridded temperature field over the Northeast for the past 200 years. We successfully reconstruct historical climate anomalies, including the 1816 'year without summer', and the warm winter and spring of 1828 (Figure 6; Ludlum, 1966; Mock et al., 2007). We use ombrotrophic AWC sites to reconstruct an area-averaged precipitation for Southern New England (Figure 8), and improve reconstructions of JJA PDSI along the coast of New England (Figure 10). This coastal PDSI field reconstruction provides new information on coastal versus inland drought patterns and the influence of Atlantic Ocean on coastal climate. In addition, our coastal tree-ring network and strong correlations with local SSTs (Figure 4) and winter Atlantic Ocean atmospheric pressure patterns (Figure 7) provides a new information source on Atlantic ocean-atmosphere dynamics.

Improved paleoclimate reconstructions in the Northeast will depend on continued development of long (prior to the 1800's) temperature sensitive tree-ring chronologies. Although AWC remains one of the most temperature sensitive species in the region (Alexander et al., 2019; Hopton & Pederson, 2005), the inclusion of multiple species in the northern part of their range limit into a temperature reconstruction may enhance our ability to extend further in time and improve our skill across a wider geographic extent (Alexan-

der et al., 2019). The reconstructions presented here confirm the anomalous nature of current temperature and drought trends in the Northeast in the context of the past few centuries. Although a common feature in the past (Figure 11), periods of sustained aridity accompanied by cold temperatures across most of the Northeast have not occurred since the 1960's (Pederson et al., 2013; Seager et al., 2012). Coupled patterns evident from the past may shift in the future, however, with regional trends toward both warmer temperatures and increased moisture due to anthropogenic greenhouse gas emission, but internal variability in the region will continue to be an important component of regional climate anomalies.

Data Availability

The data that support the findings of this study are available within the article's supplementary materials and will be openly available in The International Tree-Ring Data Bank (ITRDB) at `https://www.ncdc.noaa.gov/data-access/paleoclimatology-data/datasets/tree-ring`. All of the climate data used here are publicly available: The 20th Century Reanalysis data are available from NOAA-CIRES `https://www.esrl.noaa.gov/psd/data/gridded/data.20thC_ReanV2c.html` and HadISST data are available from the UK Met Office `https://www.metoffice.gov.uk/hadobs/hadisst/`.

Acknowledgments

This research is funded by the US National Science Foundation Paleo Perspectives on Climate Change program (P2C2; AGS-1304262 and AGS-1501856). The authors of this paper thank the many field assistants who helped develop the northeastern AWC network. We thank the 300 Committee Land Trust, Dartmouth National Resources Trust, Orleans Conservation Trust, Marine Biological Laboratory, Trustees of Reservations, National Park Service, U.S. Forest Service, The Nature Conservancy, and private land owners who allowed access to field sites.

References

Akaike, H. (1974). A new look at the statistical model identification. In *Selected papers of Hirotugu Akaike* (pp. 215–222). Springer.

Alexander, M. R., Pearl, J. K., Bishop, D. A., Cook, E. R., Anchukaitis, K. J., & Pederson, N. (2019). The potential to strengthen temperature reconstructions in ecoregions with limited tree line using a multispecies approach. *Quaternary Research*, *92*(2), 583-597. doi: 10.1017/qua.2019.33

Anchukaitis, K. J., Cook, E. R., Cook, B. I., Pearl, J. K., D'Arrigo, R., & Wilson, R. (2019). Coupled modes of north atlantic ocean-atmosphere variability and the onset of the little ice age. *Geophysical Research Letters*. doi: 10.1029/2019GL084350

Anchukaitis, K. J., Wilson, R., Briffa, K. R., Buntgen, U., Cook, E. R., D'Arrigo, R., ... Zorita, E. (2017). Last millennium Northern Hemisphere summer temperatures from tree rings: Part II, spatially resolved reconstructions. *Quaternary Science Reviews*, *163*, 1-22. doi: 10.1016/j.quascirev.2017.02.020

Anderson, O. D. (1976). *Time series analysis and forecasting: the Box-Jenkins approach*. Butterworth.

Ballinger, T. J., Allen, M. J., & Rohli, R. V. (2014). Spatiotemporal analysis of the January Northern Hemisphere circumpolar vortex over the contiguous United States. *Geophysical Research Letters*, *41*(10), 3602–3608.

Bartlett, H. H. (1909). The submarine Chamaecyparis bog at Woods Hole, Massachusetts. *Rhodora*, *11*(132), 221–235.

Belmecheri, S., Babst, F., Wahl, E. R., Stahle, D. W., & Trouet, V. (2016). Multi-century evaluation of Sierra Nevada snowpack. *Nature Climate Change*, *6*(1), 2.

Berg, N., & Hall, A. (2017). Anthropogenic warming impacts on California snowpack during drought. *Geophysical Research Letters*, *44*(5), 2511–2518.

Boswijk, G., Fowler, A., Palmer, J., Fenwick, P., Hogg, A., Lorrey, A., & Wunder, J. (2014). The late Holocene kauri chronology: assessing the potential of a 4500-year record for palaeoclimate reconstruction. *Quaternary Science Reviews*, *90*, 128–142.

Bretherton, C., Smith, C., & Wallace, J. (1992). An intercomparison of methods for finding coupled patterns in climate data. *Journal of Climate*, *5*, 541-560.

Briffa, K., & Melvin, T. (2011). A closer look at regonal curve standardization of tree-ring records: Justification of the need, a warning of some pitfalls, and suggested improvements in its application. *Dendroclimatology*, *5*.

Brown, P. J., Bradley, R. S., & Keimig, F. T. (2010). Changes in extreme climate indices for the northeastern United States, 1870–2005. *Journal of Climate*, *23*(24), 6555–6572.

Bunn, A. G., Salzer, M. W., Anchukaitis, K. J., Bruening, J. M., & Hughes, M. K. (2018). Spatiotemporal variability in the climate growth response of high elevation bristlecone pine in the White Mountains of California. *Geophysical Research Letters*, *45*(24), 13–312.

Chenoweth, M. (1996). Ships' logbooks and "the year without a summer". *Bulletin of the American Meteorological Society*, *77*(9), 2077–2094.

Collins, M. (2009). Evidence for changing flood risk in New England since the late 20th century. *Journal of the American Water Resources Association*, *45*(2), 279-290.

Compo, G. P., Whitaker, J. S., Sardeshmukh, P. D., Matsui, N., Allan, R. J., Yin, X., ... Brönnimann, S. (2011). The twentieth century reanalysis project. *Quarterly Journal of the Royal Meteorological Society*, *137*(654), 1–28.

Conkey, L. (1979). *Dendroclimatology in the Northeastern United States* (Unpublished master's thesis). University of Arizona.

Conkey, L. (1986). Red spruce tree-ring widths and densities in eastern North America as indicators of past climate. *Quaternary Research*, *26*, 232-243.

Cook, B. I., Ault, T. R., & Smerdon, J. E. (2015). Unprecedented 21st century drought risk in the American Southwest and Central Plains. *Science Advances*, *1*(1), e1400082.

Cook, B. I., Cook, E. R., Anchukaitis, K. J., Seager, R., & Miller, R. L. (2011). Forced and unforced variability of twentieth century North American droughts and pluvials. *Climate Dynamics*, *37*(5-6), 1097–1110.

Cook, B. I., Cook, E. R., Smerdon, J. E., Seager, R., Williams, A. P., Coats, S., ... Díaz, J. V. (2016). North American megadroughts in the Common Era: reconstructions and simulations. *Wiley Interdisciplinary Reviews: Climate Change*, *7*(3), 411–432.

Cook, E. (1985). *A Time Series Approach to Tree-Ring Standardization* (Unpub-

lished doctoral dissertation). University of Arizona, Tucson, AZ.

Cook, E., D'Arrigo, R. D., & Mann, M. (2002). A well-verified, multiproxy reconstruction of the winter North Atlantic Oscillation index since AD 1400. *Journal of Climate*, *15*, 1754-1764.

Cook, E., & Jacoby, G. (1977). Tree-ring -drought relationships in the Hudson Valley, NY. *Science*, *198*, 399-402.

Cook, E., & Krusic, P. (2004). *The North American Drought Atlas. Lamont-Doherty Earth Observatory and the National Science Foundation.*

Cook, E., & Krusic, P. (2012). The North American Drought Atlas. Lamont-Doherty Earth Observatory and the National Science Foundation http://iridl. ldeo. columbia. edu/SOURCES/. LDEO/. TRL. *NADA2004/. pdsi-atlas. html*.

Cook, E., Meko, D., Stahle, D., & Cleaveland, M. (1999). Drought reconstructions for the continental United States. *Journal of Climate*, *12*, 1145-1162.

Cook, E., & Peters, K. (1981). The smoothing spline: a new approach to standardizing forest interior tree-ring width series for dendroclimatic studies. *Tree-Ring Bulletin*, *41*, 45-53.

Cook, E., & Peters, K. (1997). Calculating unbiased tree-ring indices for the study of climatic and environmental change. *Holocene*, *7*, 361-370.

Cook, E. R., Anchukaitis, K. J., Buckley, B. M., D'Arrigo, R. D., Jacoby, G. C., & Wright, W. E. (2010). Asian monsoon failure and megadrought during the last millennium. *Science*, *328*(5977), 486–489.

Cook, E. R., Briffa, K. R., Meko, D. D., Graybill, D. A., & Funkhouser, G. (1995). The 'segment length curse' in long tree-ring chronology development for palaeoclimatic studie. *The Holocene*, *5*(2229-237).

Cook, E. R., Kushnir, Y., Smerdon, J. E., Williams, A. P., Anchukaitis, K. J., & Wahl, E. R. (2019). A Euro-Mediterranean tree-ring reconstruction of the winter NAO index since 910 CE. *Climate Dynamics*, 1–14.

Cook, E. R., & Pederson, N. (2011). Uncertainty, emergence, and statistics in dendrochronology. In *Dendroclimatology* (pp. 77–112). Springer.

Cook, E. R., Seager, R., Cane, M. A., & Stahle, D. W. (2007). North American drought: Reconstructions, causes, and consequences. *Earth-Science Reviews*, *81*(1-2), 93–134.

Cook, E. R., Seager, R., Heim Jr, R. R., Vose, R. S., Herweijer, C., & Woodhouse,

C. (2010). Megadroughts in North America: Placing IPCC projections of hydroclimatic change in a long-term palaeoclimate context. *Journal of Quaternary Science*, *25*(1), 48–61.

Cook, G. H. (1857). Art. xxv.–on a subsidence of the land on the sea-coast of New Jersey and Long Island. *American Journal of Science and Arts (1820-1879)*, *24*(72), 341.

Crawford, E. R., Day, F. P., & Atkinson, R. B. (2007). Influence of environment and substrate quality on root decomposition in naturally regenerating and restored Atlantic white cedar wetlands. *Wetlands*, *27*(1), 1–11.

Drake, L. (1971). Evidence for ablation and basal till in east-central New Hampshire. In *Till, a symposium* (pp. 73–91).

Enfield, D., Mestas-Nunez, A., & Trimble, P. (2001). The Atlantic Multidecadal Oscillation and its relationship to rainfall and river flows in the continental U.S. *Geophysical Research Letters*, *2001*, 2077-2080.

Esper, J. (2005). Effect of scaling and regression on reconstructed temperature amplitude for the past millennium. *Geophysical Research Letters*, *32.7*.

Esper, J., Cook, E. R., & Schweingruber, F. H. (2002). Low-frequency signals in long tree-ring chronologies for reconstructing past temperature variability. *Science*, *295*, 2250-2253.

Feng, D., Beighley, E., Hughes, R., & Kimbro, D. (2016). Spatial and temporal variations in eastern US hydrology: responses to global climate variability. *JAWRA Journal of the American Water Resources Association*, *52*(5), 1089–1108.

Findell, K., & Delworth, T. (2010). Impact of common sea surface temperature anomalies on global drought and pluvial frequency. *Journal of Climate*, *23*(3), 485-503.

Fischer, E. M., & Knutti, R. (2015). Anthropogenic contribution to global occurrence of heavy-precipitation and high-temperature extremes. *Nature Climate Change*, *5*(6), 560.

Fritts, H. (1976). *Tree rings and climate*. New York: Academic Press.

Gengarelly, L., & Lee, T. (2006). Dynamics of Atlantic white-cedar populations at a northern New England coastal wetland. *Natural Areas Journal*, *1*, 5-16.

Gleba, P. (1978). *Massachusetts mineral and fossil localities: Cambridge, Mas-*

sachusetts. Krueger Enterprises.

Golet, F. C., & Lowry, D. J. (1987). Water regimes and tree growth in Rhode Island Atlantic white cedar swamps.

Goosse, H. (2017). Reconstructed and simulated temperature asymmetry between continents in both hemispheres over the last centuries. *Climate Dynamics*, *48*(5-6), 1483–1501.

Graumlich, L. (1999). Response of tree growth to climatic variation in the mixed conifer and deciduous forests of the upper great-lakes region. *Canadian Journal of Forest Research*, *25*, 223-34.

Griffin, D., & Anchukaitis, K. J. (2014). How unusual is the 2012–2014 California drought? *Geophysical Research Letters*, *41*(24), 9017–9023.

Groisman, P. Y., Knight, R. W., Karl, T. R., Easterling, D. R., Sun, B., & Lawrimore, J. H. (2004). Contemporary changes of the hydrological cycle over the contiguous united states: Trends derived from in situ observations. *Journal of Hydrometeorology*, *5*(1), 64–85.

Grudd, H., Briffa, K. R., Karlén, W., Bartholin, T. S., Jones, P. D., & Kromer, B. (2002). A 7400-year tree-ring chronology in northern Swedish Lapland: natural climatic variability expressed on annual to millennial timescales. *The Holocene*, *12*(6), 657–665.

Harington, C. R. (1992). *The year without a summer?: World climate in 1816* (Vol. 576). Canadian Museum of Nature Ottawa.

Harris, I., Jones, P. D., Osborn, T. J., & Lister, D. H. (2014). Updated high-resolution grids of monthly climatic observations–the CRU TS3. 10 Dataset. *International journal of climatology*, *34*(3), 623–642.

Herweijer, C., Seager, R., Cook, E. R., & Emile-Geay, J. (2007). North american droughts of the last millennium from a gridded network of tree-ring data. *Journal of Climate*, *20*(7), 1353–1376.

Heusser, C. (1949). A note on buried cedar logs at Secaucus, NJ. *Bulletin of the Torrey Botanical Club*, *76*(4), 305–306.

Holmes, R. (1983). Computer-assisted quality control in tree-ring dating and measurement. *Tree-Ring Bulletin*, *43*, 69-75.

Hopton, M., & Pederson, N. (2005). Climate sensitivity of Atlantic white cedar at its northern range limit. In M. K. Burke & P. Sheridan (Eds.), *Atlantic White*

Cedar: Ecology, Resoration, and Management. Southern Research Station, Asheville, NC: USDA-Forest Service.

Horton, R., Yohe, G., Easterling, W., Kates, R., Ruth, M., Sussman, E., ... Lipschultz, F. (2014). Northeast. In J. M. Melillo, T. T. Richmond, & G. W. Yohe (Eds.), (p. 1-24). Stop IDCC, Washington DC 20402-0001: U.S. Government Printing Office.

Howarth, M. E., Thorncroft, C. D., & Bosart, L. F. (2019, mar). Changes in extreme precipitation in the Northeast United States: 1979–2014. *Journal of Hydrometeorology*.

Hu, Q., Feng, S., & Oglesby, R. J. (2011). Variations in North American summer precipitation driven by the Atlantic Multidecadal Oscillation. *Journal of Climate*, *24*(21), 5555–5570.

Huang, H., Winter, J. M., Osterberg, E. C., Horton, R. M., & Beckage, B. (2017). Total and extreme precipitation changes over the Northeastern United States. *Journal of Hydrometeorology*, *18*(6), 1783–1798.

Janowiak, M. K., D'Amato, A. W., Swanston, C. W., Iverson, L., Thompson, F. R., Dijak, W. D., ... others (2018). New England and northern New York forest ecosystem vulnerability assessment and synthesis: a report from the New England climate change response framework project. *Gen. Tech. Rep. NRS-173. Newtown Square, PA: US Department of Agriculture, Forest Service, Northern Research Station. 234 p.*, *173*, 1–234.

Jenkin, G., & Watts, D. G. (1968). Spectral analysis and its applications. *Holden Day, San Francisco*, *968*, 121.

Jones, P., Davies, T., Lister, D., Slonosky, V., Jónsson, T., Bärring, L., ... others (1999). Monthly mean pressure reconstructions for Europe for the 1780–1995 period. *International Journal of Climatology: A Journal of the Royal Meteorological Society*, *19*(4), 347–364.

Karl, T. R., & Knight, R. W. (1998). Secular trends of precipitation amount, frequency, and intensity in the United States. *Bulletin of the American Meteorological society*, *79*(2), 231–242.

Kelsey, R. G., Joseph, G., & McWilliams, M. G. (2011). Ethanol synthesis by anoxic root segments from five cedar species relates to their habitat attributes but not their known differences in vulnerability to phytophthora lateralis root disease.

Canadian journal of forest research, *41*(6), 1202–1211.

Kretschmer, M., Coumou, D., Agel, L., Barlow, M., Tziperman, E., & Cohen, J. (2018, jan). More-persistent weak stratospheric polar vortex states linked to cold extremes. *Bulletin of the American Meteorological Society*, *99*(1), 49–60.

Kunkel, K. E., Andsager, K., & Easterling, D. R. (1999). Long-term trends in extreme precipitation events over the conterminous united states and canada. *Journal of climate*, *12*(8), 2515–2527.

Kunkel, K. E., Stevens, L. E., Stevens, S. E., Sun, L., Janssen, E., Wuebbles, D., ... Dobson, J. G. (2013). Regional Climate Trends and Scenarios for the U.S. National Climate Assessment: Part 1. Climate of the Northeast U.S. *NOAA Technical Report NESDIS*, 87.

Laderman, A. (1989). The ecology of Atlantic white cedar wetlands: A community profile. *Fish and Wildlife Service Biological Report*, *85*, 125.

Laderman, A. D. (1981). *Algal ecology of a Chamaecyparis thyoides bog: An in situ microcosm study.* (Unpublished doctoral dissertation). State University of New York at Binghamton.

Laidig, K. J., & Zampella, R. A. (1999). Community attributes of Atlantic white cedar (Chamaecyparis thyoides) swamps in disturbed and undisturbed pinelands watersheds. *Wetlands*, *19*(1), 35–49.

Lamarche, V. C. (1974). Frequency-dependent relationships between tree-ring series along an ecological gradient and some dendroclimatic implications.

Limaye, V. S., Vargo, J., Harkey, M., Holloway, T., & Patz, J. A. (2018). Climate change and heat-related excess mortality in the Eastern USA. *EcoHealth*, *15*(3), 485–496.

Little, E. L. (1978). *Digital Representations of Tree Species Range Maps from Atlas of United States Trees* (Tech. Rep.). US Forest Service.

Little, S., & Garrett, P. W. (1990). Chamaecyparis thyoides (L.) BSP Atlantic white-cedar. *Silvics of North America*, *1*, 103–108.

Ludlum, D. M. (1966). *Early American winters: 1821-1870* (No. 2). American Meteorological Society.

Marlon, J. R., Pederson, N., Nolan, C., Goring, S., Shuman, B., Robertson, A., ... others (2017). Climatic history of the northeastern United States during the past 3000 years. *Climate of the Past*, *13*(10), 1355–1379.

Maxwell, R. S., Harley, G. L., Maxwell, J. T., Rayback, S. A., Pederson, N., Cook, E. R., ... Rayburn, J. A. (2017). An interbasin comparison of tree-ring reconstructed streamflow in the eastern United States. *Hydrological Processes*, *31*(13), 2381–2394.

Meko, D. (1997). Dendroclimatic reconstruction with time varying predictor subsets of tree indices. *Journal of Climate*, *10*, 687-696.

Meko, D., Cook, E. R., Stahle, D. W., Stockton, C. W., & Hughes, M. K. (1993). Spatial patterns of tree-growth anomalies in the United States and southeastern Canada. *Journal of Climate*, *6*(9), 1773–1786.

Meko, D., Touchan, R., & Anchukaitis, K. (2011). Seascorr: A MATLAB program for identifying the seasonal climate signal in an annual tree-ring time series. *Computers and Geosciences*, *27.9*, 1234-1241.

Melvin, T., & Briffa, K. (2008). A"signal-free" approach to dendroclimatic standardisation. *Dendrochronologia*, *26*(2), 71-86.

Michaelson, J. (1987). Cross-validation in statistical climate forecast models. *Journal of Climate and Applied Meteorology*, *26*, 1589-1600.

Min, S.-K., Zhang, X., Zwiers, F. W., & Hegerl, G. C. (2011). Human contribution to more-intense precipitation extremes. *Nature*, *470*(7334), 378.

Mock, C. J., Mojzisek, J., McWaters, M., Chenoweth, M., & Stahle, D. W. (2007). The winter of 1827–1828 over eastern North America: a season of extraordinary climatic anomalies, societal impacts, and false spring. *Climatic change*, *83*(1-2), 87–115.

Motzkin, G. (1990). *Age Structure and Successional Status of the Marconi Atlantic White Cedar Swamp, Cape Cod National Seashore, So, Wellfleet, Massachusetts* (Unpublished master's thesis). University of Massachusetts, Amherst.

Mulligan, A., & Uchupi, E. (2003). New interpretation of glacial history of Cape Cod may have important implications for groundwater contaminant transport. *Eos, Transactions American Geophysical Union*, *84*(19), 177–183.

Mylecraine, K. A., Kuser, J. E., Smouse, P. E., & Zimmermann, G. L. (2004). Geographic allozyme variation in Atlantic white-cedar, Chamaecyparis thyoides (cupressaceae). *Canadian Journal of Forest Research*, *34*, 2443-2454.

Mylecraine, K. A., Kuser, J. E., Zimmermann, G. L., & Smouse, P. E. (2005).

Rangewide provenance variation in Atlantic white-cedar (Chamaecyparis thyoides): early survival and growth in New Jersey and North Carolina plantations. *Forest Ecology and Management*, *216*(1-3), 91–104.

Namias, J. (1966). Nature and possible causes of the Northeastern United States drought during 1962–65. *Mon. Wea. Rev*, *94*(9), 543–554.

Namias, J. (1967). Further studies of drought over Northeastern United States. *Monthly Weather Review*, *9*(8).

Namias, J. (1983). Some causes of United States drought. *Journal of Climate and Applied Meteorology*, *22*(1), 30–39.

Newby, P. E., Shuman, B. N., Donnelly, J. P., Karnauskas, K. B., & Marsicek, J. (2014, June). Centennial-to-millennial hydrologic trends and variability along the North Atlantic Coast, USA, during the Holocene. *Geophysical Research Letters*, *41*(12), 4300–4307.

NHESP. (2007). *Natural Community Fact Sheet: Atlantic White Cedar Swamps.* Commonwealth of Massachusetts Division of Fisheries and Wildlife.

Osborn, T., Barichivich, J., Harris, I., van der Schrier, G., & Jones, P. (2017). Monitoring global drought using the self-calibrating Palmer Drought Severity Index. *Bulletin of the American Meteorological Society*, *98*(8), S32–S33.

Osborn, T. J., Briffa, K., & Jones, P. D. (1997). Adjusting variance for sample-size. *Dendrochronologia*, 89-99.

Palmer, W. C. (1965). Meteorological drought. Research Paper No. 45. Washington, DC: US Department of Commerce. *Weather Bureau*, 59.

Pearl, J. K., Anchukaitis, K. J., Pederson, N., & Donnelly, J. P. (2017). Reconstructing Northeastern United States temperatures using Atlantic white cedar tree rings. *Environmental Research Letters*, *12*(11), 114012.

Pederson, N., Bell, A., Cook, E., Lall, U., Devineni, N., Seager, R., ... Vranes, K. (2013). Is an epic pluvial masking the water insecurity of the greater New York city region. *Journal of Climate*, *26*, 1339-1354.

Pederson, N., Cook, E., Jacoby, G., Peteet, D., & Griffin, K. (2004a). The influence of winter temperatures on the annual radial growth of six northern range margin tree species. *Dendrochronologia*, *22*, 7-29.

Pederson, N., Cook, E. R., Jacoby, G. C., Peteet, D. M., & Griffin, K. L. (2004b). The influence of winter temperatures on the annual radial growth of six north-

ern range margin tree species. *Dendrochronologia*, *22*, 7-29.

Pederson, N., Tackett, K., McEwan, R. W., Clark, S., Cooper, A., Brosi, G., ... Stockwell, R. D. (2012). Long-term drought sensitivity of trees in second-growth forests in a humid region. *Canadian Journal of Forest Research*, *42*(10), 1837–1850.

Percival, D., & Constantine, W. (2006). Exact simulation of gaussian time series from nonparametric spectral estimates with application to bootstrapping. *Statistical Computing*, *16*(1), 25-35.

Percival, D. B., Walden, A. T., et al. (1993). *Spectral analysis for physical applications*. cambridge university press.

Phipps, S. J., McGregor, H. V., Gergis, J., Gallant, A. J., Neukom, R., Stevenson, S., ... Van Ommen, T. D. (2013). Paleoclimate data–model comparison and the role of climate forcings over the past 1500 years. *Journal of Climate*, *26*(18), 6915–6936.

Rampino, M. R., & Self, S. (1982). Historic eruptions of Tambora (1815), Krakatau (1883), and Agung (1963), their stratospheric aerosols, and climatic impact. *Quaternary Research*, *18*(2), 127–143.

Rayner, N. A., Parker, D., Horton, E., Folland, C., Alexander, L., Rowell, D. P., ... Kaplan, A. (2003). Global analyses of sea surface temperature, sea ice, and night marine air temperature since the late nineteenth century. *Geophysical Research Letters*, *108*(D14).

Rodgers, H. L., Day, F. P., & Atkinson, R. B. (2003). Fine root dynamics in two atlantic white-cedar wetlands with contrasting hydroperiods. *Wetlands*, *23*(4), 941–949.

Roig Jr, F., Roig, C., Rabassa, J., & Boninsegna, J. (1996). Fuegian floating tree-ring chronology from subfossil Nothofagus wood. *The Holocene*, *6*(4), 469–476.

Salzer, M. W., & Hughes, M. K. (2007). Bristlecone pine tree rings and volcanic eruptions over the last 5000 yr. *Quaternary Research*, *67*(1), 57–68.

Salzer, M. W., Pearson, C. L., & Baisan, C. H. (2019). Dating the methuselah walk bristlecone pine floating chronologies. *Tree-Ring Research*.

Schneider, U., Becker, A., Finger, P., Meyer-Christoffer, A., Rudolf, B., & Ziese, M. (2015). GPCC full data reanalysis version 7.0 at 0.5 °: Monthly land-surface

precipitation from rain-gauges built on gts-based and historic data. *Global Precipitation Climatology Centre*.

Schneider, U., Becker, A., Finger, P., Meyer-Christoffer, A., Rudolf, B., & Ziese, M. (2016). GPCC Full Data Reanalysis Version 7.0: Monthly Land-Surface Precipitation from Rain Gauges built on GTS based and Historic Data. *Global Precipitation Climatology Center*.

Seager, R., Pederson, N., Kushnir, Y., Nakamura, J., & Jurburg, S. (2012). The 1960s drought and the subsequent shift to a wetter climate in the Catskill mountains region of the New York City watershed. *Journal of Climate*, *25*(19), 6721-6742.

Snee, R. D. (1977). Validation of regression models: methods and examples. *Technometrics*, *19*(4), 415–428.

St George, S., & Ault, T. R. (2014). The imprint of climate within Northern Hemisphere trees. *Quaternary Science Reviews*, *89*, 1–4.

Stahle, D., Fye, F., Cook, E., & Griffin, R. (2007). Tree-ring reconstructed megadroughts. *Climatic Change*, *83*, 133-149.

Stahle, D. W., & Cleaveland, M. K. (1992). Reconstruction and analysis of spring rainfall over the southeastern US for the past 1000 years. *Bulletin of the American Meteorological Society*, *73*(12), 1947–1961.

Stokes, M., & Smiley, T. (1968). *An Introduction to Tree-Ring Dating*. Chicago, IL: University of Chicago Press.

Stothers, R. B. (1984). The great Tambora eruption in 1815 and its aftermath. *Science*, *224*(4654), 1191–1198.

Sweet, S. K., Wolfe, D. W., DeGaetano, A., & Benner, R. (2017). Anatomy of the 2016 drought in the northeastern United States: implications for agriculture and water resources in humid climates. *Agricultural and Forest Meteorology*, *247*, 571–581.

Trettin, C. C., Jurgensen, M. F., Grigal, D. F., Gale, M. R., & Jeglum, J. R. (1996). *Northern forested wetlands ecology and management*. CRC Press.

Trouet, V., Diaz, H., Wahl, E., Viau, A., Graham, R., Graham, N., & Cook, E. (2013). A 1500-year reconstruction of annual mean temperature for temperate North America on decadal-to-multidecadal time scales. *Environmental Research Letters*, *8*(2), 024008.

Wahl, E., & Ammann, C. (2007). Robustness of the mann, bradley, hughes reconstruction of northern hemisphere surface temperatures: Examination of criticisms based on the nature and processing of proxy climate evidence. *Climatic Change*, *85*(1-2), 33-69.

Wahl, E., & Smerdon, J. (2012). Comparative performance of paleoclimate field and index reconstructions derived from climate proxies and noise-only predictors. *Geophysical Research Letters*.

Wallace, J., Smith, C., & Bretherton, C. (1992). Singular value decomposition of wintertime sea surface temperature and 500-mb height anomalies. *Journal of Climate*, *5*(6), 561-576.

Wells, N., Goddard, S., & Hayes, M. J. (2004). A self-calibrating Palmer drought severity index. *Journal of Climate*, *17*(12), 2335–2351.

Wettstein, J., & Mearns, L. (2002). The Influence of the North Atlantic Arctic Oscillation on Mean , Variance , and Extremes of Temperature in the Northeastern United States and Canada. *Journal of Climate*, *15*(24), 3586-3600.

Wigley, T. (1984). On the average value of correlated time series, with applications in dendroclimatology and hydrometeorology. *Journal of Climate and Applied Meteorology*, *23*(201-213).

Wilson, R., Anchukaitis, K., Briffa, K., Büntgen, U., Cook, E., D'Arrigo, R., ... Zorita, E. (2016). Last millennium northern hemisphere summer temperatures from tree rings: Part I: The long term context. *Quaternary Science Reviews*, *134*, 1-18.

Wilson, R., Loader, N., Rydval, M., Patton, H., Frith, A., Mills, C., ... Gunnarson, B. E. (2012). Reconstructing Holocene climate from tree rings: The potential for a long chronology from the Scottish Highlands. *The Holocene*, *22*(1), 3–11.

Yamaguchi, D. (1990). A simple method for cross-dating increment cores from living trees. *Canadian Journal of Forest Research*, *21*(414-416).

Table 1. Atlantic white cedar sites retained for climate reconstructions. Numbers correspond to site locations in Figure 1.

Site Name	State	Site Code	Lat Lon (°N °W)	Elev. (m)	# Trees	Time Span	Hydrologic Designation
1. Acushnet Swamp	MA	ACU	41.685 -70.962	18	25	1841-2015	Hydrologically Stable
2. Appleton Bog	ME	APB	44.333 -69.272	100	33	1859-2014	Hydrologically Stable
3. Bellvale Mountain	NJ	BVC	41.206 -74.326	353	50	1845-2015	Drought Prone
4. Black Pond Bog	MA	BLK	42.181 -70.812	38	23	1799-2015	Hydrologically Stable
5. Brown Mill Pond	NH	TFT	42.987 -70.782	10	21	1813-2015	Drought Prone
6. Buck Island Rd.	MA	OFS	41.662 -70.256	2	21	1817-2015	Drought Prone
7. Destruction Brook	MA	DBR	41.575 -71.018	25	27	1850-2015	Drought Prone
8. Ell Pond	RI	ELL	41.507 -71.780	99	21	1866-2015	Drought Prone
9. Grinnell Swamp	MA	GNL	41.448 -70.754	1	41	1813-2014	Ombrotrophic
10. Hosea's Swamp	MA	HOS	41.747 -69.979	1	22	1828-2015	Ombrotrophic
11. Lake Tonnetta	NY	MAF	41.426 -73.612	164	22	1852-2015	Hydrologically Stable
12. Marconi National Seashore	MA	MRC	41.910 -69.981	0-4	53	1802-2014	Ombrotrophic
13. Marine Biological Laboratory 1	MA	MBL1	41.527 -70.654	2	21	1761-2014	Ombrotrophic
14. Marine Biological Laboratory 2	MA	MBL2	41.524 -70.656	3	22	1804-2015	Ombrotrophic
15. Mashpee Pine Barrens	MA	MPB	41.590 -70.489	3	30	1790-2014	Hydrologically Stable
16. Massabessic Experimental Forest	ME	TLH	43.447 -70.674	93	22	1846-2016	Hydrologically Stable
17. North Madison Forest	CT	CAF	41.3646 -72.65	94	48	1814-2015	Hydrologically Stable
18. Orealans Swamp	MA	ORS	41.755 -69.977	0	21	1854-2015	Ombrotrophic
19. Saco Heath Bog	ME	SAC	43.548 -70.466	45	27	1872-2014	Hydrologically Stable
20. Sagg Swamp	NY	SAG	40.936 -72.285	6	21	1907-2015	Hydrologically Stable
21. Uttertown	NJ	CBJ	41.115 -74.42	343	42	1764-2015	Drought Prone
22. Walpole Cedar Swamp	MA	UTF	42.110 -71.271	57	21	1873-2015	Hydrologically Stable
23. West Hill Dam	MA	WHD	42.104 -72.612	80	21	1883-2015	Drought Prone
24. Westminster Swamp	MA	WMS	42.526 -71.948	335	30	1845-2014	Hydrologically Stable

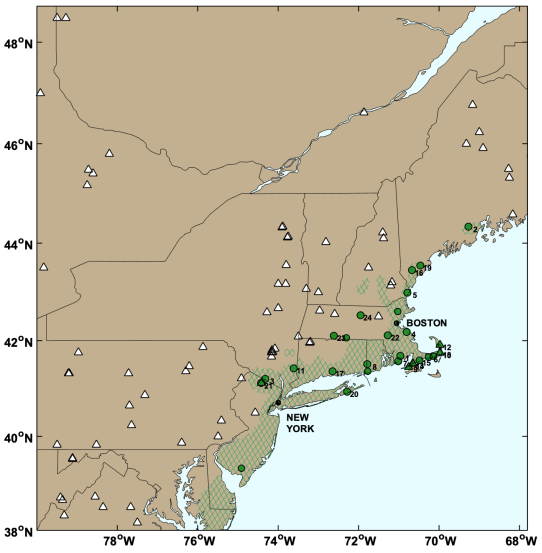

Figure 1. Location of collected Atlantic White Cedar (AWC) sites (green – this study). Site numbers correspond to those in Table 1. Ombrotrophic AWC sites are marked as green triangles, all other AWC sites are marked as green circles. Green hatching indicates the species distribution as defined by the United States Forest Service (E. L. Little, 1978). Location of tree-ring chronologies that are used in the North American Drought Atlas are marked as white triangles (E. R. Cook, Seager, et al., 2010).

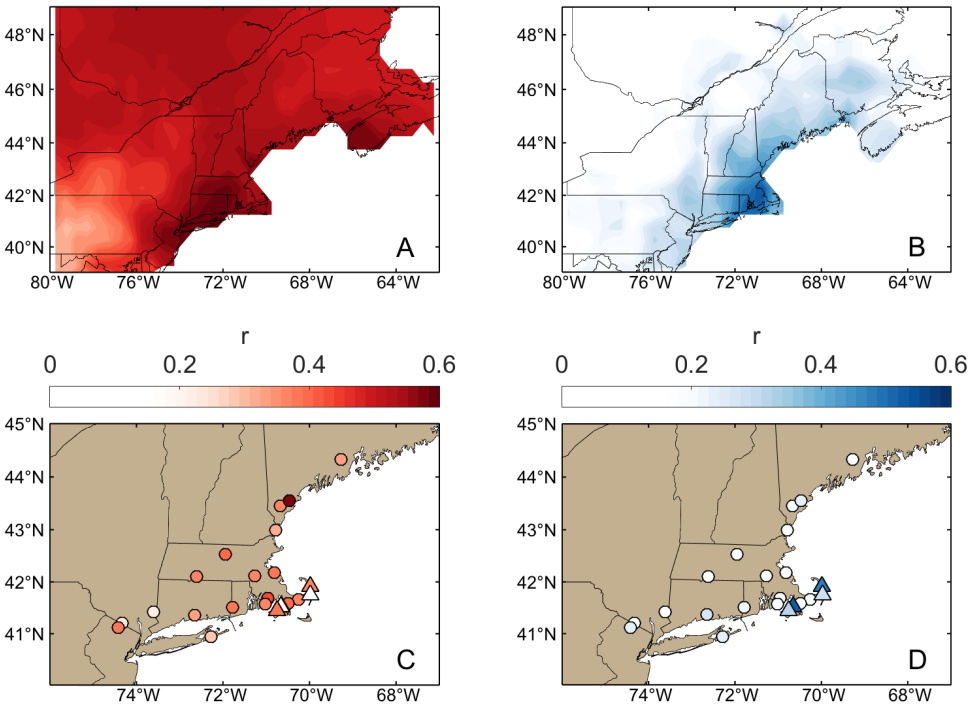

Figure 2. (A) Field correlation (Pearson's) of the temperature sensitive AWC network's EOF1 signal with January-August mean temperature (Harris et al., 2014). (B) Field correlation of the ombrotrophic AWC network's EOF1 signal with March-August mean precipitation (Schneider et al., 2015). (C) Individual site correlations with local grid point temperature (Harris et al., 2014). Ombrotrophic sites are marked as triangles. Hydrologically stable and drought prone sites are marked as circles. Color of the symbol refers to the strength of the correlation. (D) Individual site correlations with local grid point precipitation (Schneider et al., 2015). Ombrotrophic sites are marked as triangles. Hydrologically stable and drought prone sites are marked as circles. Color of the symbol refers to the strength of the correlation. Colorscale is the same for panel A,C, and B, D respectively.

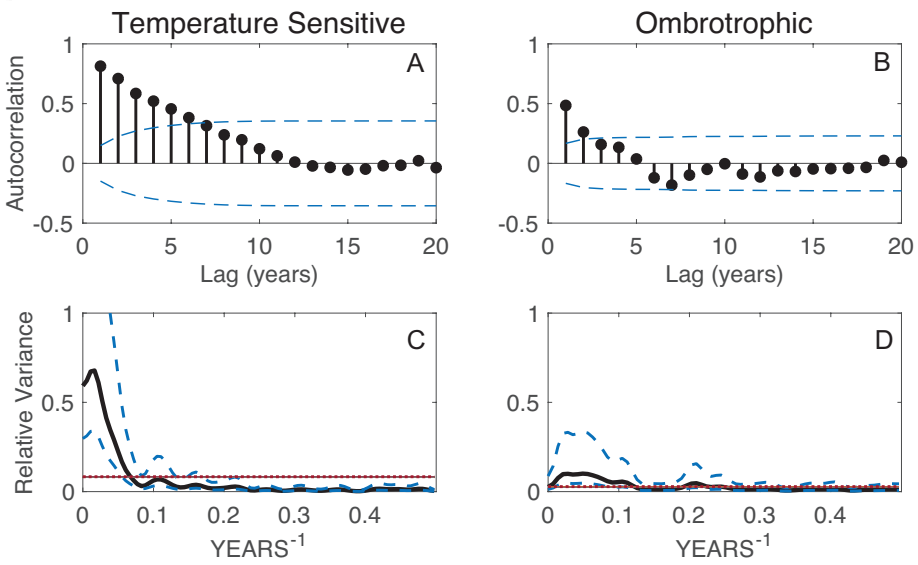

Figure 3. Autocorrelation and spectral properties of chronologies. Lagged autocorrelation of (A) a representative temperature sensitive site (MPB), and (B) representative ombrotrophic site (HOS) without the 21^{st} century trend. Blue dashed lines are the large-lag standard error (Anderson, 1976). Blackman-Tukey Spectrum of the (C) MPB and (D) HOS chronologies. Thick black line is the variance of the time series, dashed blue lines are the 95% confidence intervals of the spectrum (Jenkin & Watts, 1968). The red horizontal dashed line is the null Gaussian (white) noise spectrum.

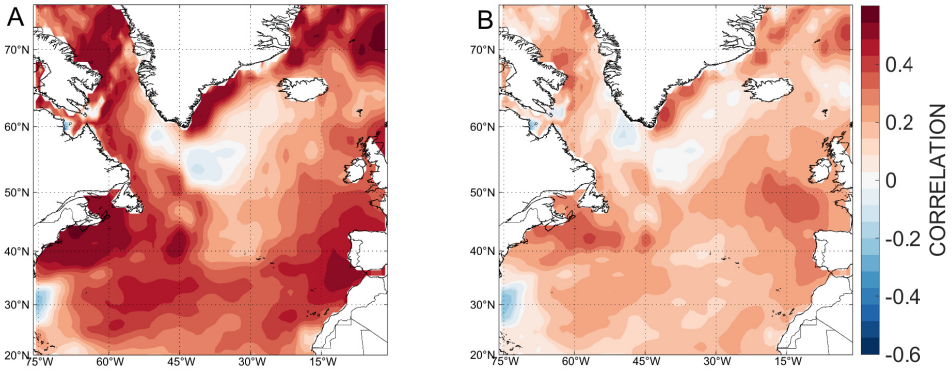

Figure 4. Correlations of temperature sensitive and ombrotrophic AWC networks with Atlantic SSTs (HADISST; Rayner et al., 2003). (A) Correlation of the temperature sensitive network's EOF1 with Atlantic SSTs. (B) Correlation of the ombrotrophic network's EOF1 with Atlantic SSTs.

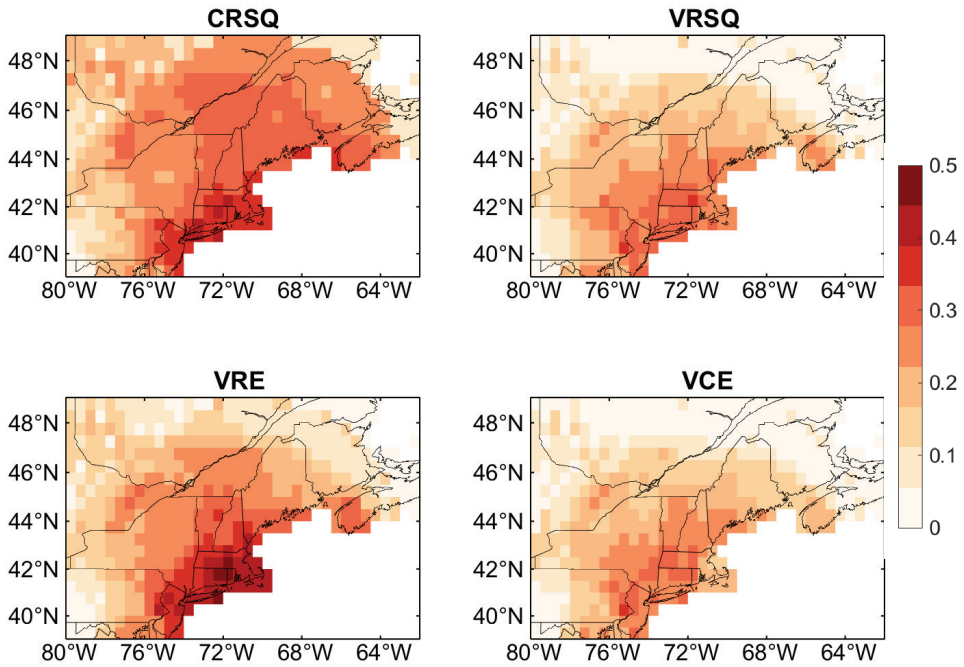

Figure 5. The maximum skill statistics for the Northeast temperature reconstruction using the AWC network. CRSQ is the final reconstruction calibration period (1900-2010) R^2, VRSQ is the validation period (1950-2010) R^2, VRE is the validation period reduction of error coefficient, VCE is the validation period coefficient of efficiency. Colors indicate the associated skill values.

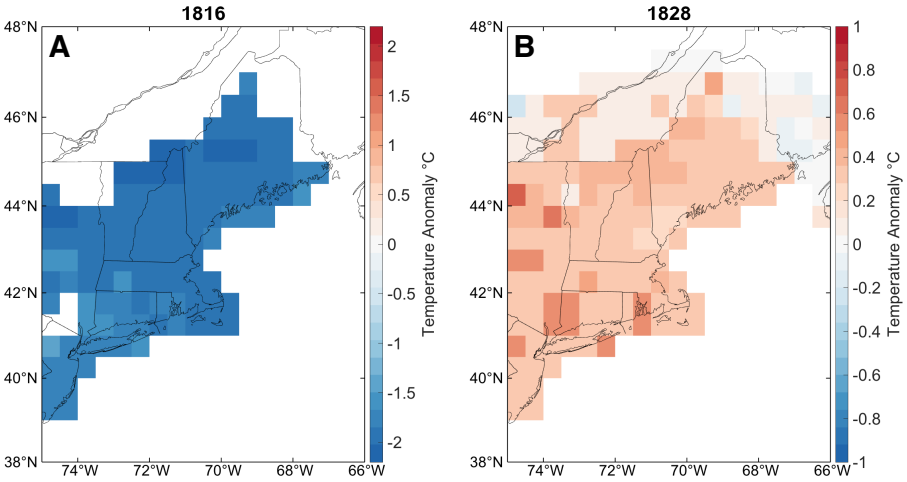

Figure 6. Reconstructed January-August mean temperature anomalies (reference period 1950-1980) for (A) 1816 (Chenoweth, 1996) and (B) 1828 (Ludlum, 1966; Mock et al., 2007). Only grid points with skillful (RE >0) temperature reconstructions are mapped.

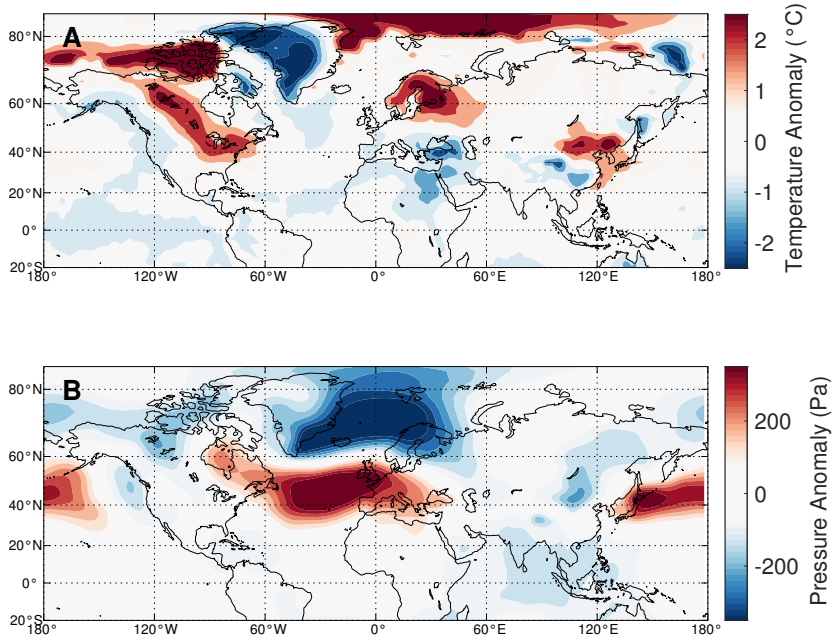

Figure 7. (A) The difference in winter (January-March) surface temperature anomalies between the reconstructed warmest years (75th percentile) and coldest years (25th percentile) in the 20th century. (B) The difference in winter (January-March) sea level pressure anomalies between the reconstructed warmest years (75th percentile) and coldest years (25th percentile) in the 20th century.

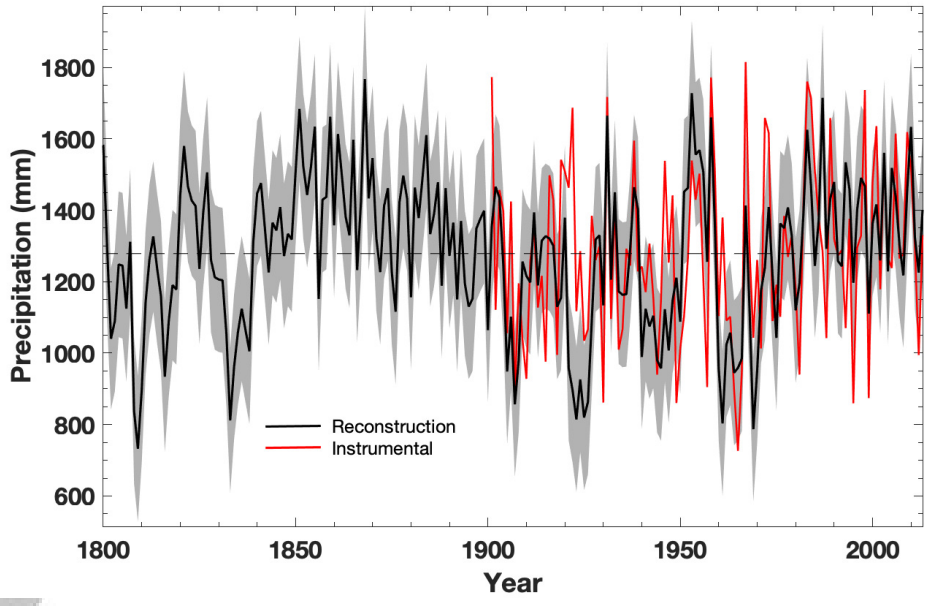

Figure 8. Nested CPS reconstruction of Southern New England March-August sum precipitation using the ombrotrophic AWC chronologies. Target instrumental data, taken from GPCC (Schneider et al., 2015) is shown in red, reconstruction record from tree-ring widths in black. The shaded uncertainty represents ± 1 RMSE of validation. Sum precipitation for the region over the 1950-1980 period is marked with a dashed line (1278mm).

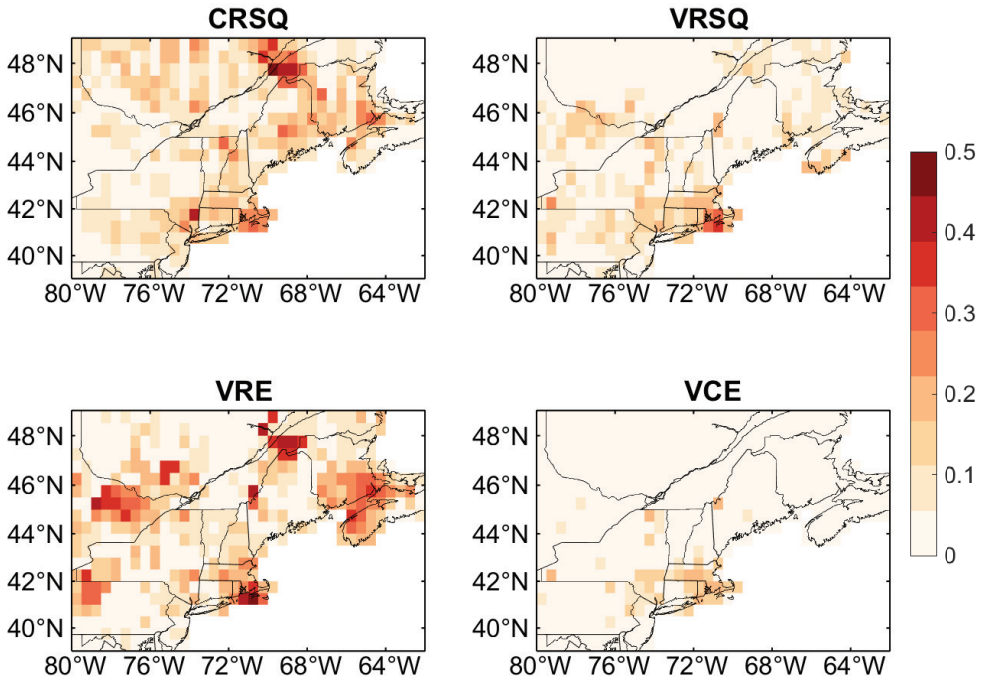

Figure 9. The maximum skill statistics for the JJA PDSI (CRU Self-calibrating Palmer Drought Severity Index (T. Osborn et al., 2017) reconstruction using just the ombrotrophic AWC sites. CRSQ is the calibration period (1900-1955) R^2, VRSQ is the validation period (1956-2010) R^2, VRE is the validation period reduction of error coefficient, VCE is the validation period coefficient of efficiency. Colors indicate the associated skill values.

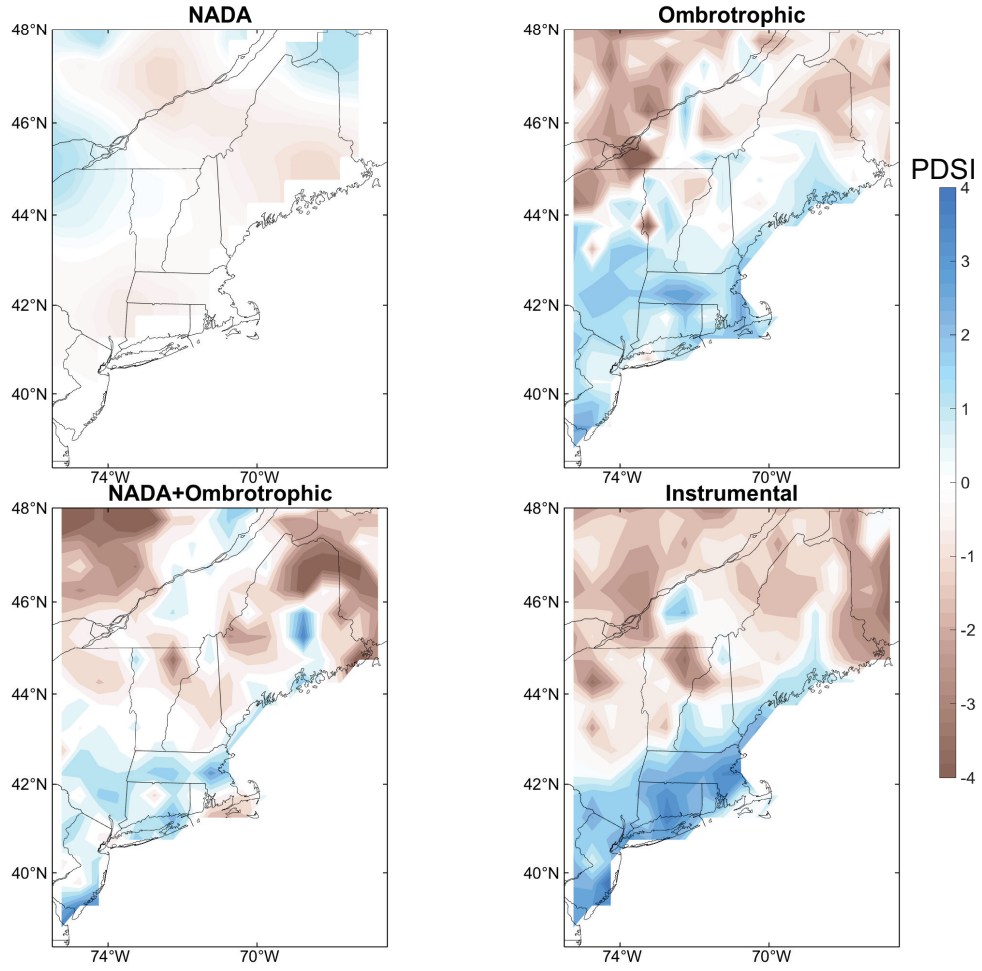

Figure 10. PDSI reconstructions and instrumental data for JJA PDSI of 1920. 'NADA': the NADA Reconstruction of 1920 JJA PDSI. 'Ombrotrophic': 1920 JJA PDSI reconstruction using only the ombrotrophic AWC sites as predictors. 'NADA+Ombrotrophic': 1920 JJA PDSI using both NADA chronologies and ombrotrophic AWC as predictors. 'Instrumental': the instrumental target field for 1920 JJA PDSI taken from the CRU Self-calibrating Palmer Drought Severity Index, where negative numbers indicate dryer than normal conditions, and positive numbers indicate wetter than normal conditions (T. Osborn et al., 2017).

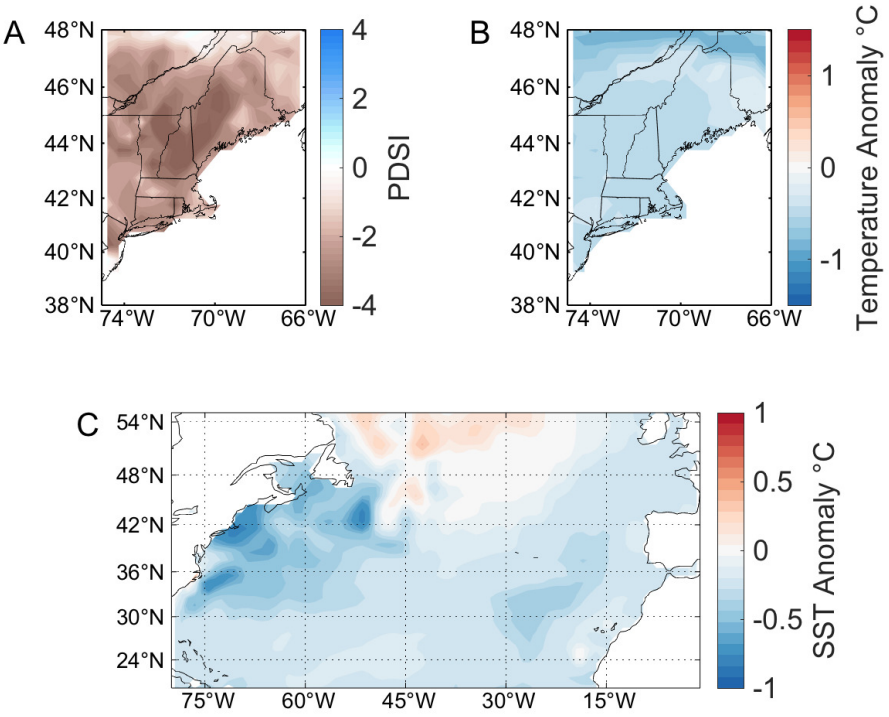

Figure 11. (A) Average PDSI for drought periods of equal or greater to the 1960's drought DAI as reconstructed by the NADA+Ombrotrophic network over the past 200 years. (B) Average land temperature anomalies (reference period 1950-1980) for drought periods of equal or greater to the 1960's drought DAI and length as reconstructed by the AWC network over the past 200 years. (C) Average Atlantic SSTs for drought periods of equal or greater to the 1960's drought DAI and length since 1870. Data from the UK Met Office Hadley Center sea surface temperature (HADISST Rayner et al., 2003)

Figure 1.

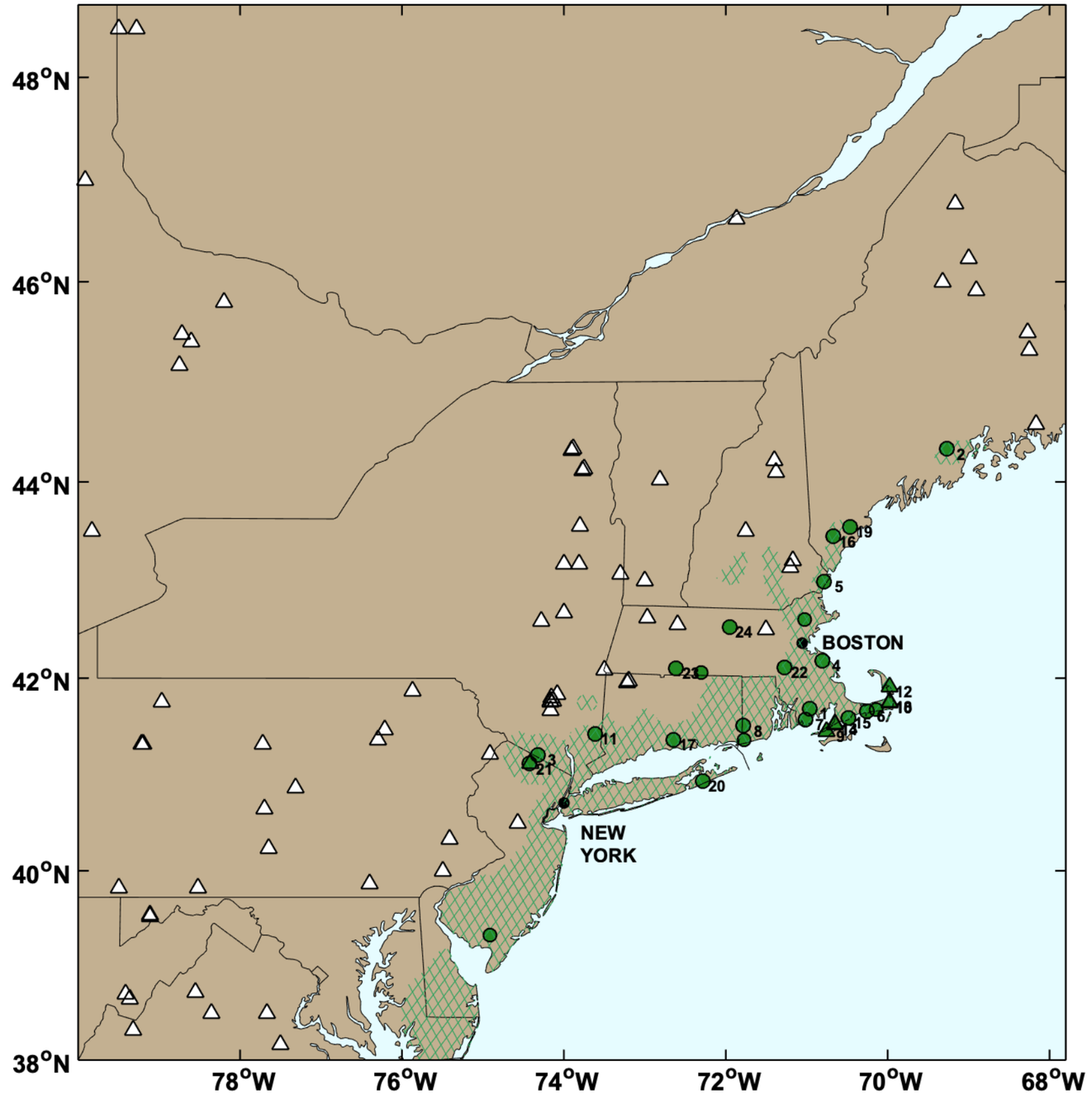

Figure 2.

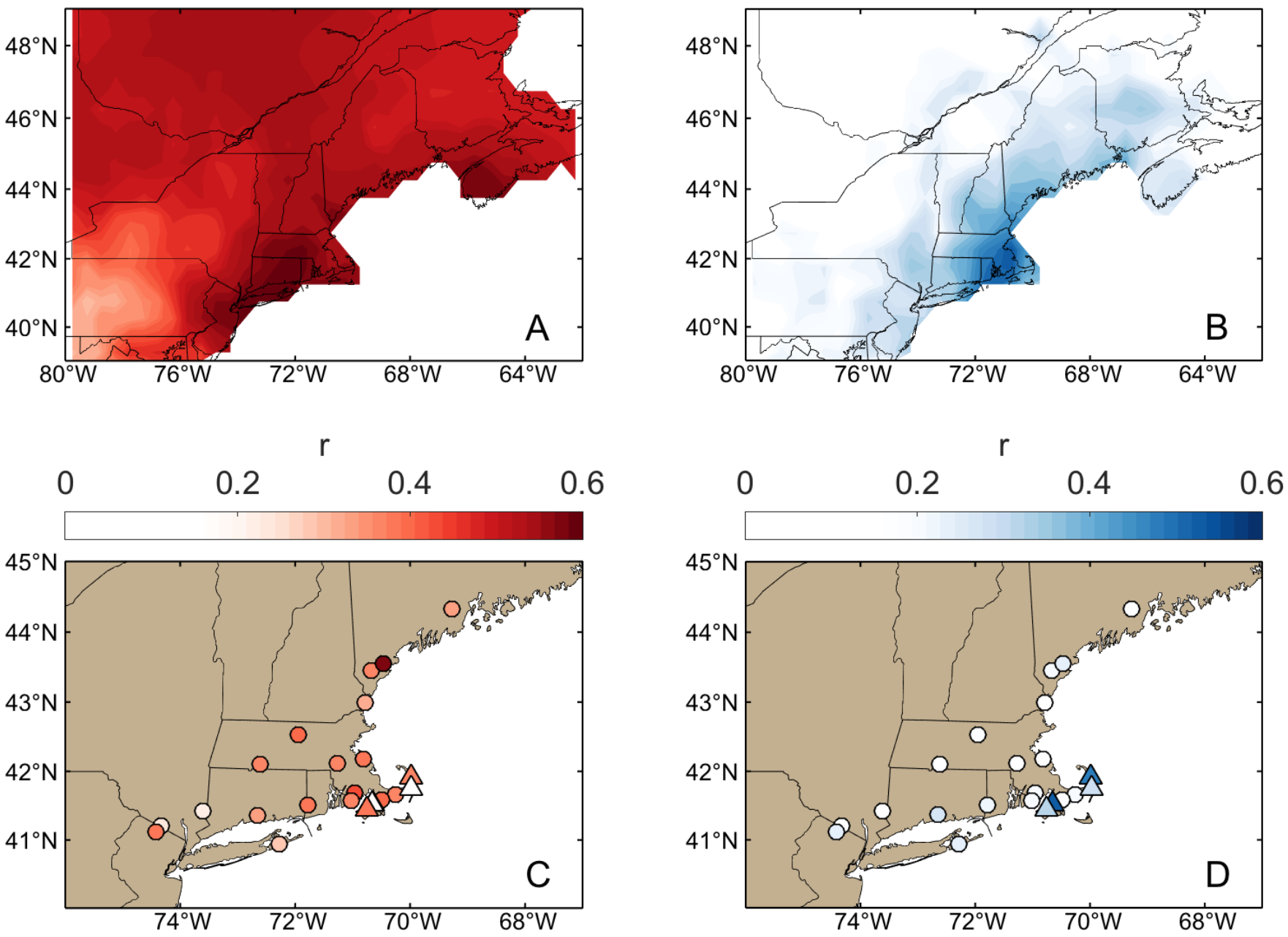

Figure 3.

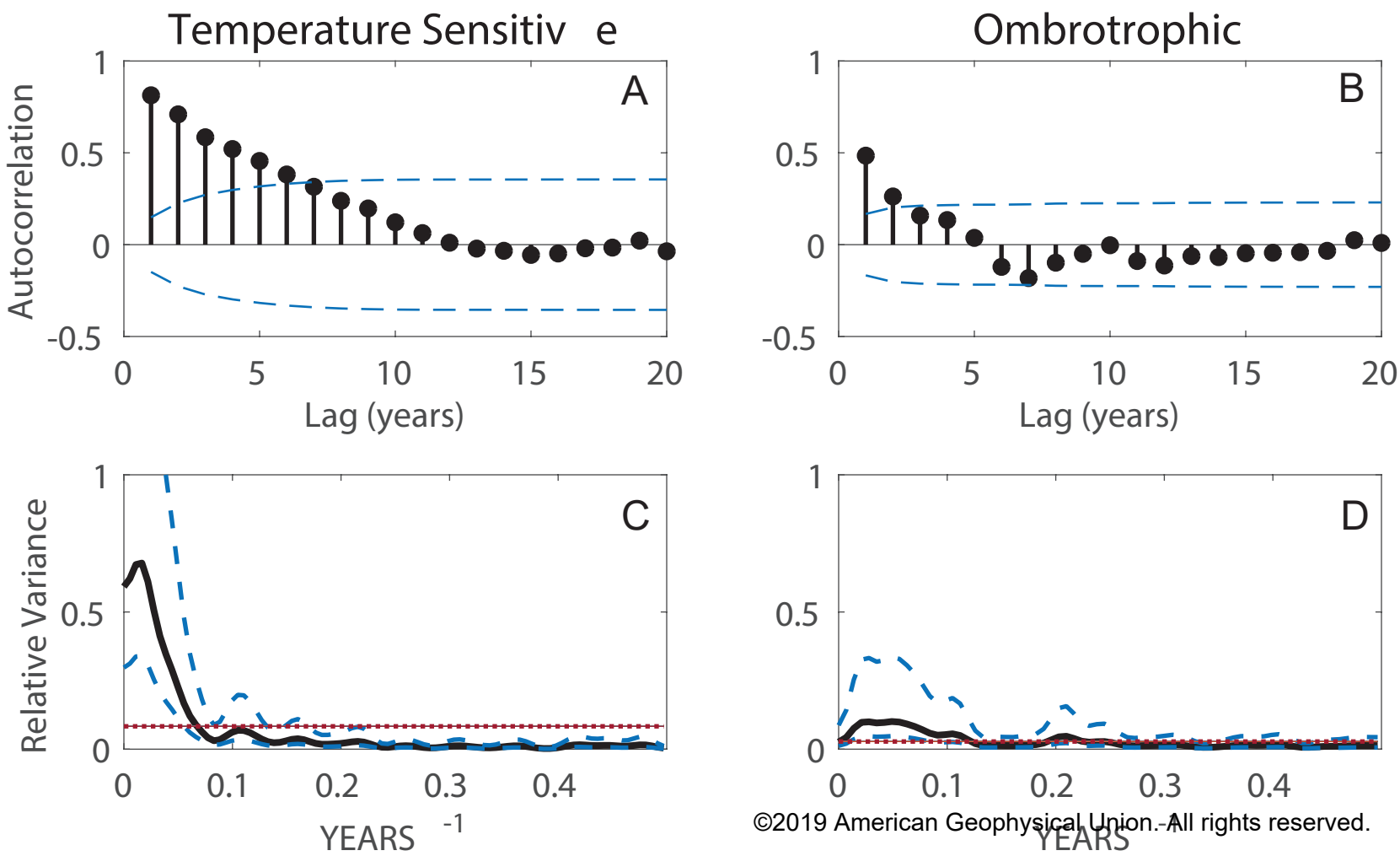

Figure 4.

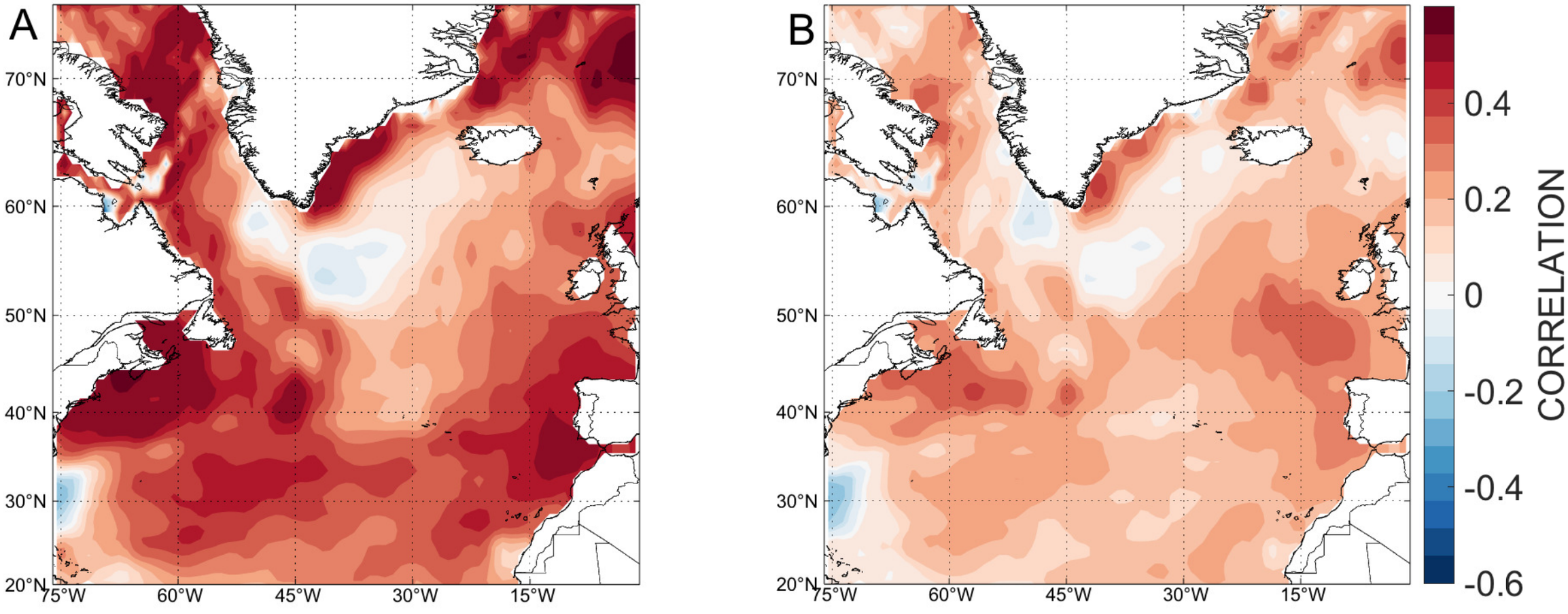

Figure 5.

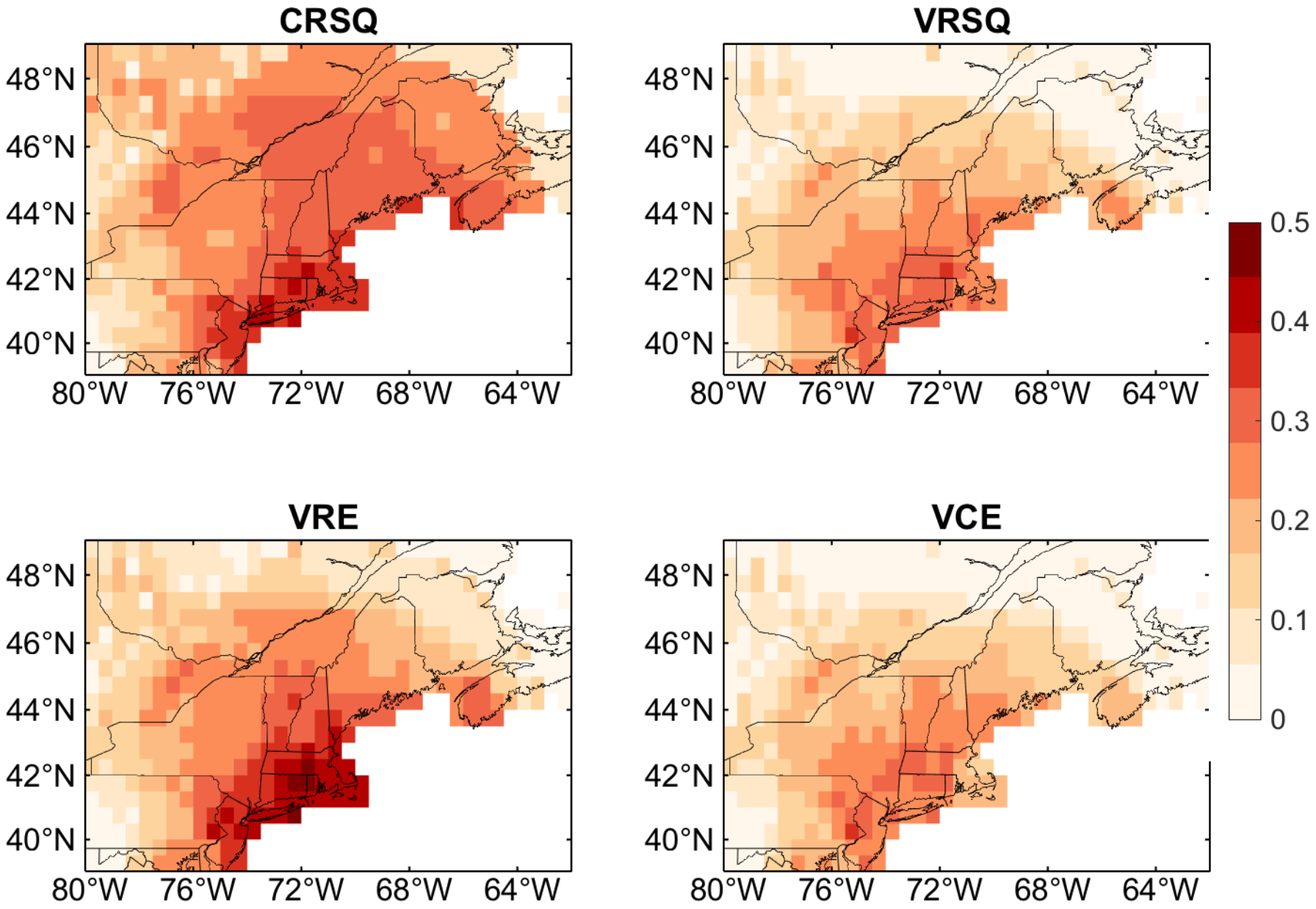

Figure 6.

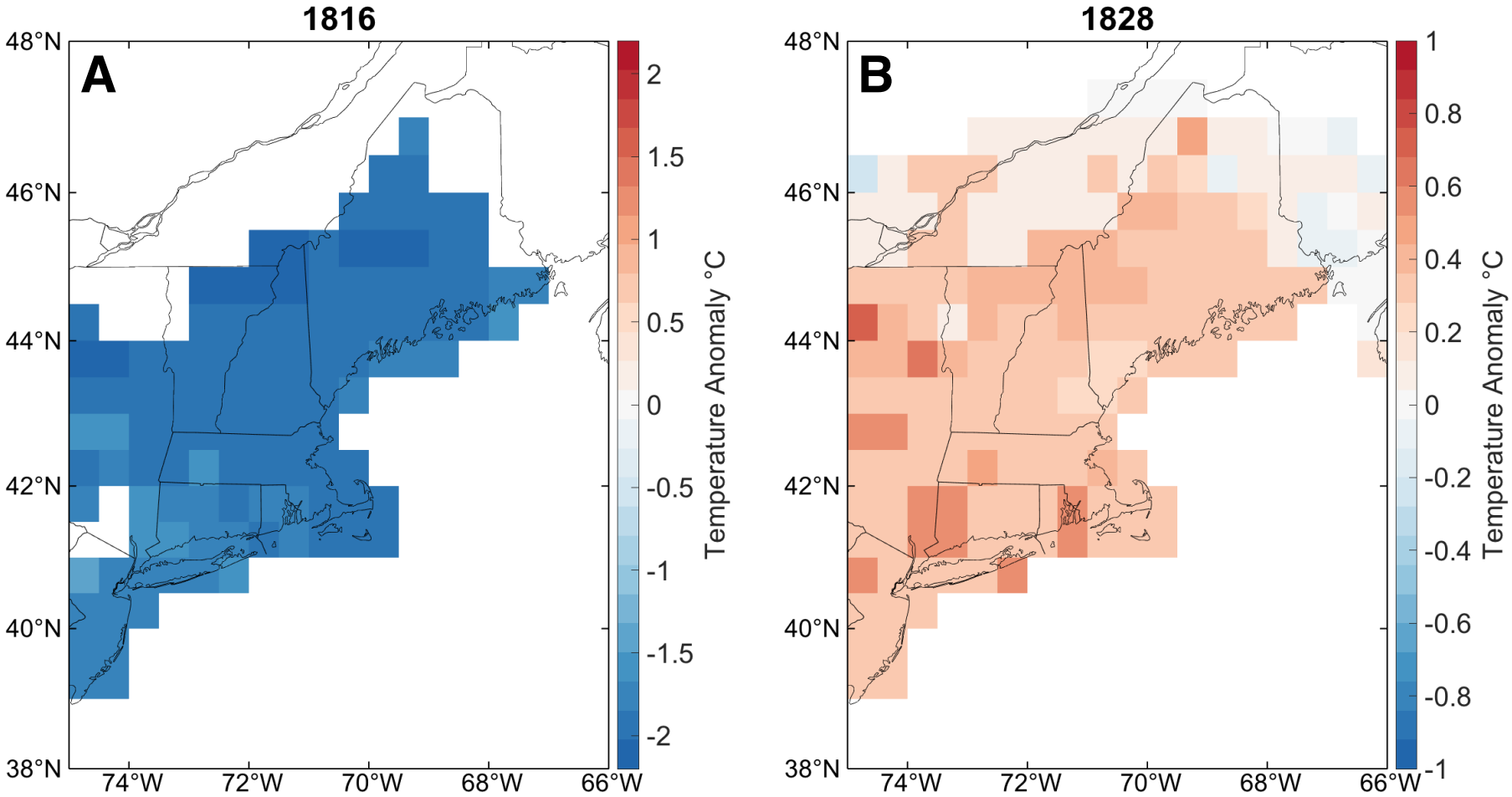

Figure 7.

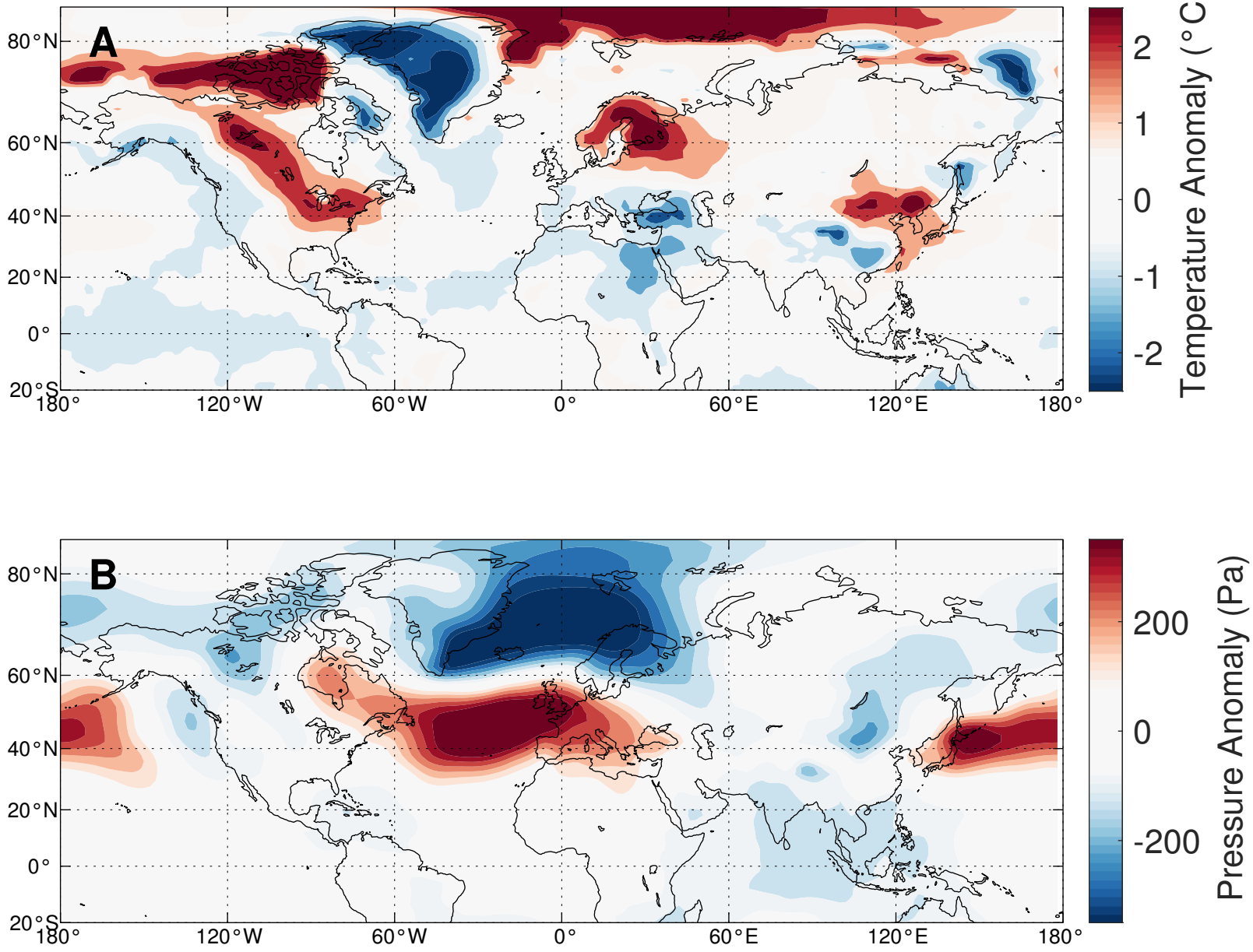

Figure 8.

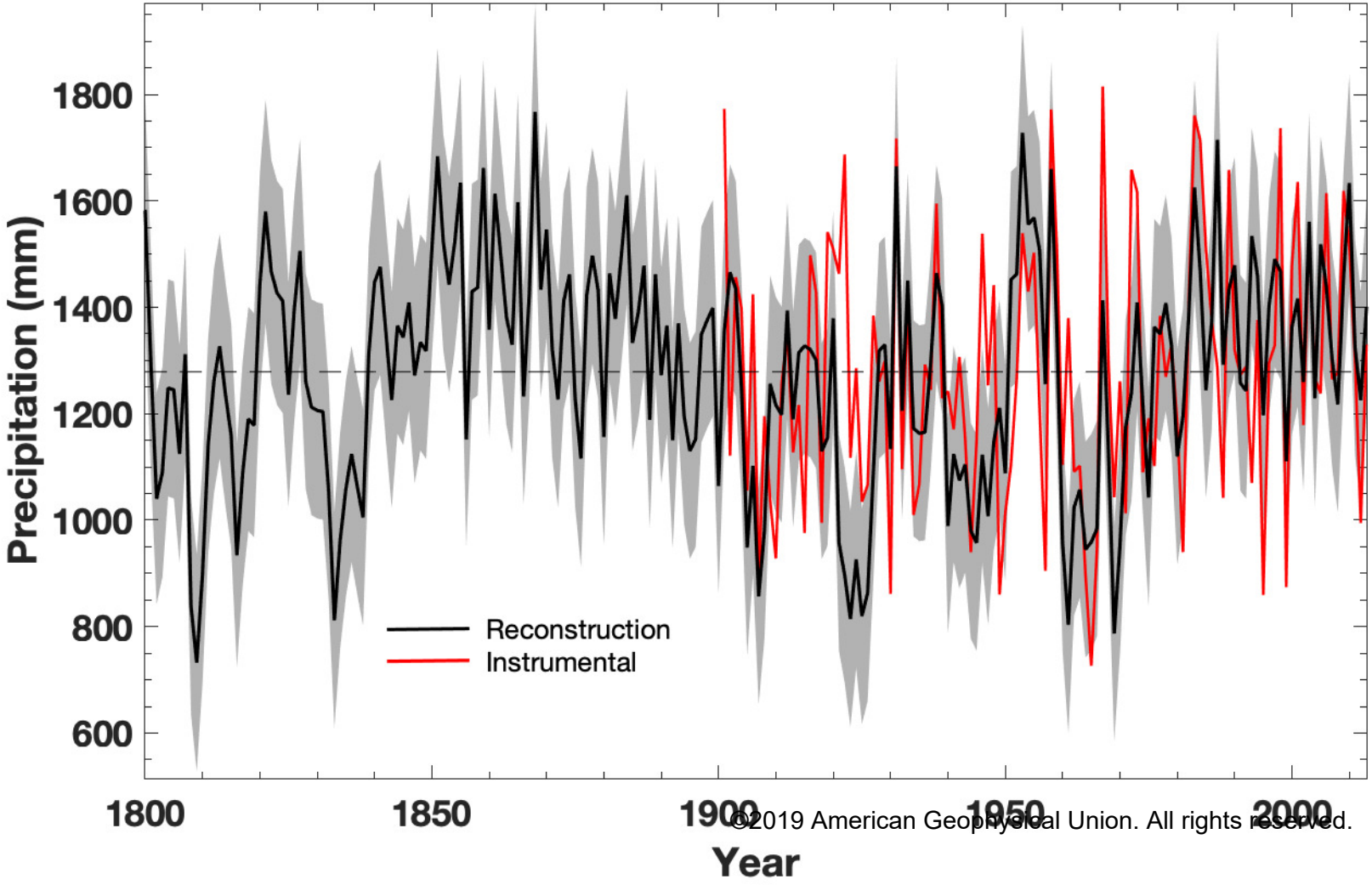

Figure 9.

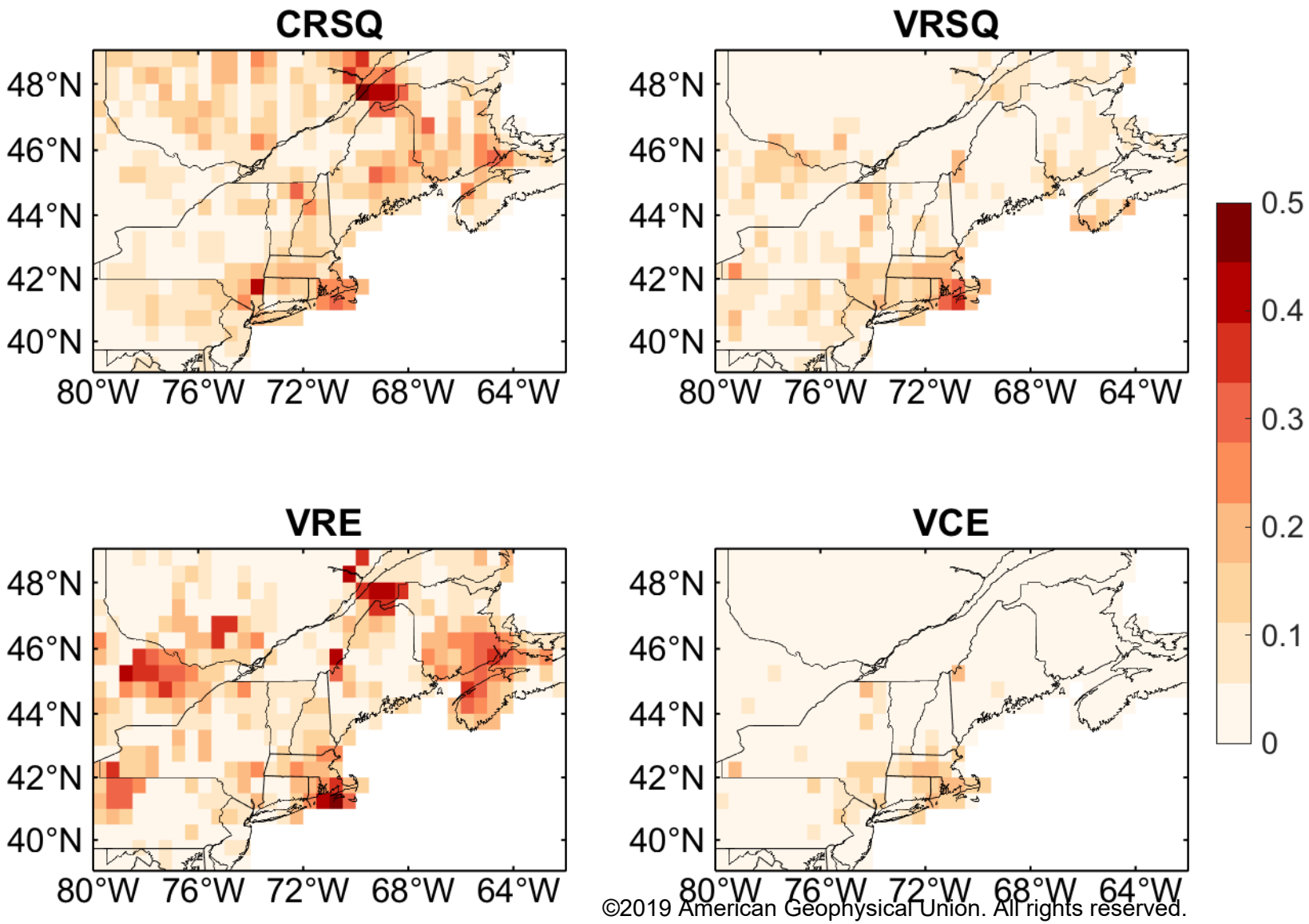

Figure 10.

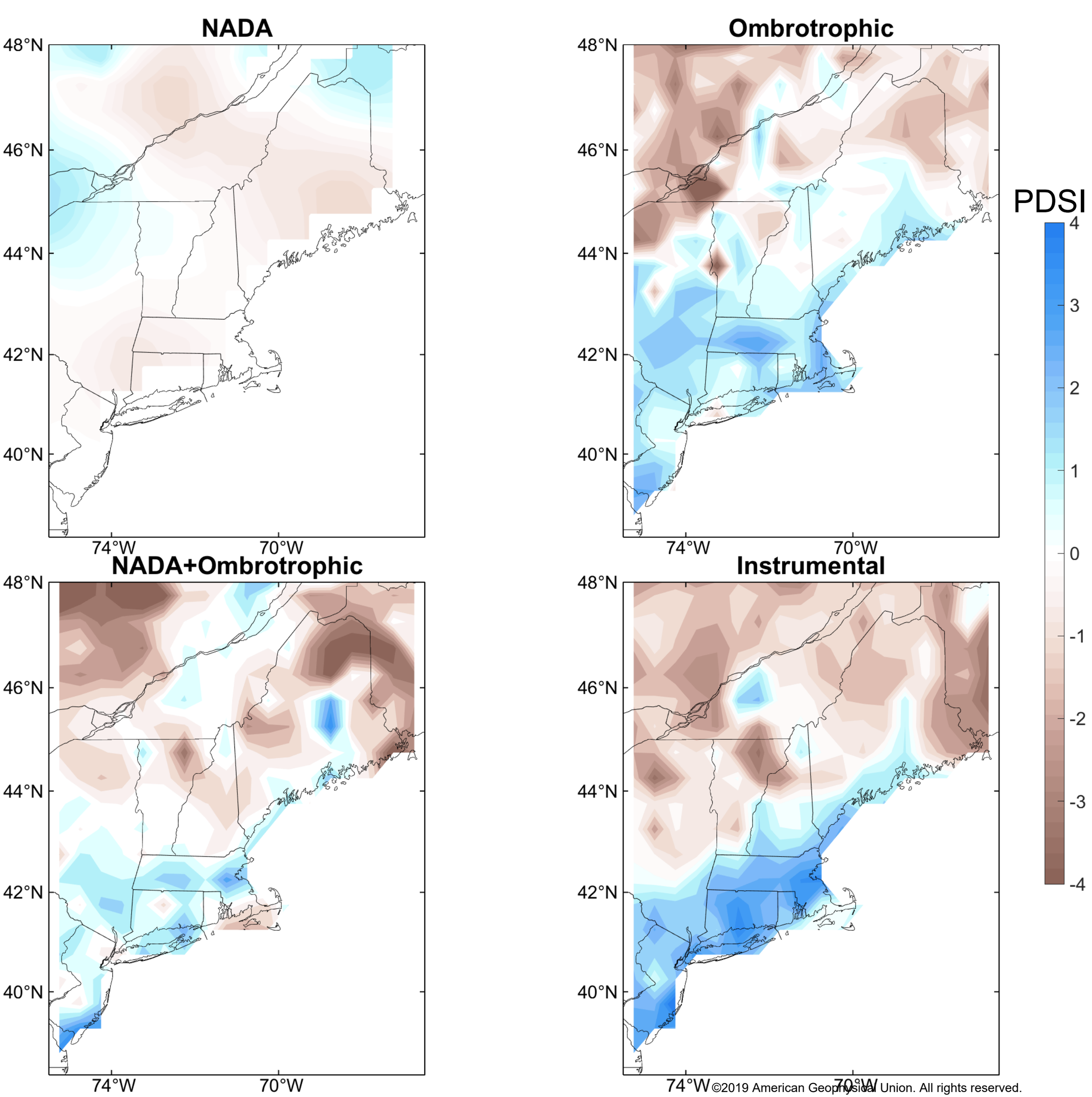

Figure 11.